measurement could result in subtracting the utterance process-related activation from the word generation-related activation, resulting in an altered lateralization of brain activation. In fact, orthographic, phonological, and semantic processing in language tasks were reported to be differentially lateralized in a fMRI study (Shaywitz et al., 1995).

The distinction between baseline CBF and activation-related changes in CBF and CBV should be stressed. The present study, as well as the studies mentioned above, examined activation-related changes in CBF and CBV using NIRS, PET, SPECT, and fMRI.

The effects of sex and age on baseline levels of CBF, CBV, and cerebral glucose metabolism measured at the resting state have been reported with rather different results from those of activation studies. Studies on sex differences in CBF, CBV, and cerebral glucose metabolism yielded variable results in the resting state as well as in the activation state. Compared with male subjects, cerebral perfusion and metabolism in female subjects were reported to be higher both in terms of global CBF (Gur et al., 1982; Rodriguez et al., 1988) and regional CBF in the temporal regions (Ragland et al., 2000), but to be lower in terms of cerebral glucose metabolism in the temporal-limbic region (Gur et al., 1995), and to be without significant difference in cerebral glucose metabolism (Azari et al., 1992). The results of these studies in the resting state should be taken into consideration when interpreting the results of activation studies: for example, increased baseline perfusion and metabolism could result in decreased activation due to the ceiling effect. However, as far as the authors surveyed, no studies that examined baseline and activation levels simultaneously in the same subjects have been carried out.

The age-dependent decrease in CBF, CBV, and cerebral glucose metabolism in the resting state as well as in the activation state, in contrast, has been frequently replicated (Marchal et al., 1992; Meltzer et al., 2000; Murphy et al., 1996; Pantano et al., 1984; Yamaguchi et al., 1986). The age-dependent decrease in cerebral perfusion and metabolism in the resting state is hypothesized to result from the combined effects of direct neuronal loss, cellular biological impairment, and functional deafferentation (Marchal et al., 1992) and such mechanisms could also underlie the age-dependent decrease in activation in terms of cerebral perfusion and metabolism.

Two limitations in the present study should be addressed. First, NIRS measures the hemoglobin concentration changes only as relative values. The estimation of hemoglobin concentration changes depends on the assumed near-infrared pathlength; hence, differences in this pathlength among the subjects could influence the obtained results. The result for age effect, at least, should be interpreted carefully because pathlength was reported to be weakly dependent on age, approximately 5% for 10 years at the most (Duncan et al., 1996), but not on sex (Duncan et al., 1995). Second, the NIRS probes employed in the present study covered only limited cerebral regions. We could not measure regional CBV over gap areas between the frontal and temporal probes as well as between the parietal and occipital areas, and the left gap area is assumed to correspond to Broca's area. Measurement of regional CBV in Broca's area could demonstrate different results regarding age, sex, and task performance dependencies. Further studies are required to address these limitations.

In conclusion, the present study demonstrated that multi-channel NIRS can detect cerebral activation during cognitive tasks and can also clarify sex- and age-dependent differences in such cerebral activation. Sex- and age-dependent differences in cerebral activation obtained in the present study should be considered when interpreting CBF, CBV, and cerebral glucose metabolism data.

Acknowledgments

This research was supported in part by a grant-in-aid for Scientific Research (C) from the Japanese Ministry of Education, Culture, Sports, Science and Technology (MF), a Health and Labour Sciences Research Grant for Research on Psychiatric and Neurological Diseases and Mental Health (MF), and a Health and Labour Sciences Research Grant for Special Research from the Japanese Ministry of Health, Labour and Welfare (MM). The authors gratefully thank Drs. Itsuro Ida, Tomohiro Suto, Makoto Ito, and Yutaka Yamagishi of the Department of Psychiatry and Human Behavior, Gunma University Graduate School of Medicine and two medical students, Mr. Ryu Takizawa and Ms. Ayako Kawakami, of the same university for their collaborations. The authors also gratefully acknowledge the assistance of Mr. Suguru Hattori in statistical analysis.

References

Azari, N.P., Rapoport, S.I., Grady, C.L., DeCarli, C., Haxby, J.V., Schapiro, M.B., et al., 1992. Gender differences in correlations of cerebral glucose metabolic rates in young normal adults. Brain Res. 574, 198–208.

Buckner, R.L., Raichle, M.E., Petersen, S.E., 1995. Dissociation of human prefrontal cortical areas across different speech production tasks and gender groups. J. Neurophysiol. 74, 2163–2173.

Chance, B., Zhuang, Z., UnAh, C., Alter, C., Lipton, L., 1993. Cognition-activated low-frequency modulation of light absorption in human brain. Proc. Natl. Acad. Sci. U. S. A. 90, 3770–3774.

Collins, D.W., Kimura, D., 1997. A large sex difference on a two-dimensional mental rotation task. Behav. Neurosci. 111, 845–849.

Duncan, A., Meek, J.H., Clemence, M., Elwell, C.E., Tyszczuk, L., Cope, M., et al., 1995. Optical pathlength measurements on adult head, calf and forearm and the head of the newborn infant using phase resolved optical spectroscopy. Phys. Med. Biol. 40, 295–304.

Duncan, A., Meek, J.H., Clemence, M., Elwell, C.E., Fallon, P., Tyszczuk, L., et al., 1996. Measurement of cranial optical path length as a function of age using phase resolved near infrared spectroscopy. Pediatr. Res. 39, 889–894.

Fallgatter, A.J., Roesler, M., Sitzmann, L., Heidrich, A., Mueller, T.J., Strik, W.K., 1997. Loss of functional hemispheric asymmetry in Alzheimer's dementia assessed with near-infrared spectroscopy. Brain Res. Cogn. Brain Res. 6, 67–72.

Frost, J.A., Binder, J.R., Springer, J.A., Hammeke, T.A., Bellgowan, P.S., Rao, S.M., et al., 1999. Language processing is strongly left lateralized in both sexes. Evidence from functional MRI. Brain 122, 199–208.

Grady, C.L., Craik, F.I., 2000. Changes in memory processing with age. Curr. Opin. Neurobiol. 10, 224–231.

Gur, R.C., Gur, R.E., Obrist, W.D., Hungerbuhler, J.P., Younkin, D., Rosen, A.D., et al., 1982. Sex and handedness differences in cerebral blood flow during rest and cognitive activity. Science 217, 659–661.

Gur, R.C., Mozley, L.H., Mozley, P.D., Resnick, S.M., Karp, J.S., Alavi, A., et al., 1995. Sex differences in regional cerebral glucose metabolism during a resting state. Science 267, 528–531.

Halpern, D.F., 2000. Sex differences in cognitive abilities, third ed. Lawrence Erlbaum Associates, Marwah, NJ.

Hazlett, E.A., Buchsbaum, M.S., Mohs, R.C., Spiegel-Cohen, J., Wei, T.C.,

Azueta, R., et al., 1998. Age-related shift in brain region activity during successful memory performance. Neurobiol. Aging 19, 437–445.
Herrmann, M.J., Ehlis, A.C., Fallgatter, A.J., 2003. Frontal activation during a verbal-fluency task as measured by near-infrared spectroscopy. Brain Res. Bull. 61, 51–56.
Hock, C., Muller-Spahn, F., Schuh-Hofer, S., Hofmann, M., Dirnagl, U., Villringer, A., 1995. Age dependency of changes in cerebral hemoglobin oxygenation during brain activation: a near-infrared spectroscopy study. J. Cereb. Blood Flow Metab. 15, 1103–1108.
Hock, C., Villringer, K., Muller-Spahn, F., Wenzel, R., Heekeren, H., Schuh-Hofer, S., et al., 1997. Decrease in parietal cerebral hemoglobin oxygenation during performance of a verbal fluency task in patients with Alzheimer's disease monitored by means of near-infrared spectroscopy (NIRS): correlation with simultaneous rCBF-PET measurements. Brain Res. 755, 293–303.
Hoshi, Y., Tamura, M., 1993. Detection of dynamic changes in cerebral oxygenation coupled to neuronal function during mental work in man. Neurosci. Lett. 150, 5–8.
Ito, Y., Kennan, R.P., Watanabe, E., Koizumi, H., 2000. Assessment of heating effects in skin during continuous wave near infrared spectroscopy. J. Biomed. Opt. 5, 383–390.
Jaeger, J.J., Lockwood, A.H., Van Valin Jr., R.D., Kemmerer, D.L., Murphy, B.W., Wack, D.S., 1998. Sex differences in brain regions activated by grammatical and reading tasks. NeuroReport 9, 2803–2807.
Kato, T., Kamei, A., Takashima, S., Ozaki, T., 1993. Human visual cortical function during photic stimulation monitoring by means of near-infrared spectroscopy. J. Cereb. Blood Flow Metab. 13, 516–520.
Kleinschmidt, A., Obrig, H., Requardt, M., Merboldt, K.D., Dirnagl, U., Villringer, A., et al., 1996. Simultaneous recording of cerebral blood oxygenation changes during human brain activation by magnetic resonance imaging and near-infrared spectroscopy. J. Cereb. Blood Flow Metab. 16, 817–826.
Koizumi, H., Yamashita, Y., Maki, A., Yamamoto, T., Ito, Y., Itagaki, H., et al., 1999. Higher-order brain function analysis by trans-cranial dynamic near-infrared spectroscopy imaging. J. Biomed. Opt. 4, 403–413.
Kwee, I.L., Nakada, T., 2003. Dorsolateral prefrontal lobe activation declines significantly with age: functional NIRS study. J. Neurol. 250, 525–529.
Maki, A., Yamashita, Y., Ito, Y., Watanabe, E., Mayanagi, Y., Koizumi, H., 1995. Spatial and temporal analysis of human motor activity using noninvasive NIR topography. Med. Phys. 22, 1997–2005.
Malonek, D., Dirnagl, U., Lindauer, U., Yamada, K., Kanno, I., Grinvald, A., 1997. Vascular imprints of neuronal activity: relationships between the dynamics of cortical blood flow, oxygenation, and volume changes following sensory stimulation. Proc. Natl. Acad. Sci. U. S. A. 95, 14826–14831.
Marchal, G., Rioux, P., Petit-Taboue, M.C., Sette, G., Travere, J.M., Le Poec, C., et al., 1992. Regional cerebral oxygen consumption, blood flow, and blood volume in healthy human aging. Arch. Neurol. 49, 1013–1020.
Matsuo, K., Kato, T., Fukuda, M., Kato, N., 2000. Alteration of hemoglobin oxygenation in the frontal region in elderly depressed patients as measured by near-infrared spectroscopy. J. Neuropsychiatry Clin. Neurosci. 12, 465–471.
Matsuo, K., Kato, N., Kato, T., 2002. Decreased cerebral haemodynamic response to cognitive and physiological tasks in mood disorders as shown by near-infrared spectroscopy. Psychol. Med. 32, 1029–1037.
Meltzer, C.C., Cantwell, M.N., Greer, P.J., Ben-Eliezer, D., Smith, G., Frank, G., et al., 2000. Does cerebral blood flow decline in healthy aging? A PET study with partial-volume correction. J. Nucl. Med. 41, 1842–1848.
Murphy, D.G., DeCarli, C., McIntosh, A.R., Daly, E., Mentis, M.J., Pietrini, P., et al., 1996. Sex differences in human brain morphometry and metabolism: an in vivo quantitative magnetic resonance imaging and positron emission tomography study on the effect of aging. Arch. Gen. Psychiatry 53, 585–594.
Obrig, H., Villringer, A., 2003. Beyond the visible: imaging the human brain with light. J. Cereb. Blood Flow Metab. 23, 1–18.
Oldfield, R.C., 1970. The assessment and analysis of handedness: the Edinburgh inventory. Neuropsychologia 9, 97–113.
Pantano, P., Baron, J.C., Lebrun-Grandie, P., Duquesnoy, N., Bousser, M.G., Comar, D., 1984. Regional cerebral blood flow and oxygen consumption in human aging. Stroke 15, 635–641.
Parks, R.W., Loewenstein, D.A., Dodrill, K.L., Barker, W.W., Yoshii, F., Chang, J.Y., 1988. Cerebral metabolic effects of a verbal fluency test: a PET scan study. J. Clin. Exp. Neuropsychol. 10, 565–575.
Ragland, J.D., Coleman, A.R., Gur, R.C., Glahn, D.C., Gur, R.E., 2000. Sex differences in brain–behavior relationships between verbal episodic memory and resting regional cerebral blood flow. Neuropsychologia 38, 451–461.
Rodriguez, G., Warkentin, S., Risberg, J., Rosadini, G., 1988. Sex differences in regional cerebral blood flow. J. Cereb. Blood Flow Metab. 8, 783–789.
Sakai, K.L., Hashimoto, R., Homae, F., 2001. Sentence processing in the cerebral cortex. Neurosci. Res. 39, 1–10.
Sato, H., Takeuchi, T., Sakai, K.L., 1999. Temporal cortex activation during speech recognition: an optical topography study. Cognition 73, B55–B66.
Schlosser, R., Hutchinson, M., Joseffer, S., Rusinek, H., Saarimaki, A., Stevenson, J., et al., 1998. Functional magnetic resonance imaging of human brain activity in a verbal fluency task. J. Neurol. Neurosurg. Psychiatry 64, 492–498.
Schroeter, M.L., Zysset, S., Kruggel, F., von Cramon, D.Y., 2003. Age dependency of the hemodynamic response as measured by functional near-infrared spectroscopy. NeuroImage 19, 555–564.
Shaywitz, B.A., Shaywitz, S.E., Pugh, K.R., Constable, R.T., Skudlarski, P., Fulbright, R.K., et al., 1995. Sex differences in the function organization of the brain for language. Nature 373, 607–609.
Silverman, I., Phillips, K., Silverman, L.K., 1996. Homogeneity of effect sizes for sex across spatial tests and cultures: implications for hormonal theories. Brain Cogn. 31, 90–94.
Strangman, G., Boas, D.A., Sutton, J.P., 2002a. Non-invasive neuroimaging using near-infrared light. Biol. Psychiatry 52, 679–693.
Strangman, G., Culver, J.P., Thompson, J.H., Boas, D.A., 2002b. A quantitative comparison of simultaneous BOLD fMRI and NIRS recordings during functional brain activation. NeuroImage 17, 719–731.
Suto, T., Fukuda, M., Ito, M., Uehara, T., Mikuni, M., 2004. Multichannel near-infrared spectroscopy in depression and schizophrenia: cognitive brain activation study. Biol. Psychiatry 55, 501–511.
Toronov, V., Webb, A., Choi, J.H., Wolf, M., Michalos, A., Gratton, E., et al., 2001. Investigation of human brain hemodynamics by simultaneous near-infrared spectroscopy and functional magnetic resonance imaging. Med. Phys. 28, 521–527.
Vikingstad, E.M., George, K.P., Johnson, A.F., Cao, Y., 2000. Cortical language lateralization in right handed normal subjects using functional magnetic resonance imaging. J. Neurol. Sci. 175, 17–27.
Villringer, A., Planck, J., Hock, C., Schleinkofer, L., Dirnagl, U., 1993. Near infrared spectroscopy (NIRS): a new tool to study hemodynamic changes during activation of brain function in human adults. Neurosci. Lett. 154, 101–104.
Watanabe, E., Maki, A., Kawaguchi, F., Takashiro, K., Yamashita, Y., Koizumi, H., et al., 1998. Non-invasive assessment of language dominance with near-infrared spectroscopic mapping. Neurosci. Lett. 256, 49–52.
Yamaguchi, F., Kanno, I., Uemura, K., Shishido, F., Inugami, A., Ogawa, T., et al., 1986. Reduction in regional cerebral metabolic rate of oxygen during human aging. Stroke 17, 1220–1228.
Yamamoto, T., Yamashita, Y., Yoshizawa, H., Maki, A., Iwata, M., Watanabe, E., et al., 1999. Non-invasive measurement of language function by using optical topography. SPIE 3597, 230–237.

Available online at www.sciencedirect.com

SCIENCE DIRECT

Molecular Brain Research 129 (2004) 20–32

MOLECULAR BRAIN RESEARCH

www.elsevier.com/locate/molbrainres

Research report

Expression profile of mRNAs from rat hippocampus and its application to microarray

Takeshi Tanaka[a], Yukio Horikawa[b,c,*], Takanori Kawamoto[a], Noriko Kabe-Sakurai[a], Jun Takeda[b,c,d], Masahiko Mikuni[a]

[a]*Department of Psychiatry and Human Behavior, Gunma University, Graduate School of Medicine, Gunma, Japan*
[b]*Laboratory of Molecular Genetics, Department of Cell Biology, Institute for Molecular and Cellular Regulation, Gunma University, Gunma, Japan*
[c]*Core Research for Evolutional Science and Technology (CREST), Japan Science and Technology Corporation (JST), Kawaguchi, Japan*
[d]*Division of Bioregulatory Medicine, Department of Endocrinology, Diabetes and Rheumatology, Gifu University School of Medicine, Gifu, Japan*

Accepted 17 June 2004
Available online 23 July 2004

Abstract

Stress refers to physiological or psychological stimuli that disrupt homeostasis and induce pathophysiological conditions due to maladaptive response, sometimes resulting in mental disorders including depression and post-traumatic stress disorder. Severe stress has been shown to induce neuronal atrophy and apoptosis, especially in the hippocampus, which is thought to be a region of the brain important in stress-related disorders. We have analyzed gene expression in rat hippocampus comprehensively to clarify the molecular mechanism of stress-related disorders. In the present study, we identified and catalogued 13,660 partial complementary DNA sequences (expressed sequence tags (ESTs)) of randomly selected clones from a cDNA library of rat hippocampus. Sequence analysis showed that these clones cluster into 7173 non-redundant sequences comprising 1794 clusters and 5379 singletons. As a result of nucleotide and peptide database search, 2594 were found to represent known rat sequences. Of the remaining 4579 genes, 599 non-redundant ESTs represent rat homologs of genes identified in other species or new members of structurally related families. In addition, we illustrate the use of these clone sets by constructing a cDNA microarray focused on genes categorized into 'cell/organism defense'. These ESTs and our own microarray thus provide an improved genomic source for molecular studies of animal models of stress-related disorders.

Theme: Cellular and molecular biology
Topic: Gene structure and function: general

Keywords: Hippocampus; Stress; Expressed sequence tags (ESTs); cDNA library; Microarray

1. Introduction

The hippocampus is not only crucial in learning and memory but also is especially vulnerable to stress. This region of the brain also is involved in feedback regulation of the hypothalamus–pituitary–adrenal axis, dysfunction of which is associated with depression [12,30]. The effects of chronic stress on brain function via CRF, ACTH, and glucocorticoids may trigger some of the pathophysiological changes in brain function related to depression and other stress-related disorders. Glucocorticoids are known to influence most brain regions, but have particularly dramatic effects on limbic structures such as hippocampus and amygdala [24]. Recent studies suggest that stress-induced atrophy and loss of hippocampal neurons may contribute to the pathophysiology of depression [6,20]. Interestingly, hippocampal volume is decreased in patients with stress-related disorders, including depression and

* Corresponding author. Laboratory of Molecular Genetics, Department of Cell Biology, Institute for Molecular and Cellular Regulation, Gunma University, 3-39-15 Showa-machi, Maebashi, Gunma 371-8512, Japan. Tel.: +81 27 220 8831; fax: +81 27 220 8889.
E-mail address: yhorikaw@showa.gunma-u.ac.jp (Y. Horikawa).

0169-328X/$ - see front matter © 2004 Elsevier B.V. All rights reserved.
doi:10.1016/j.molbrainres.2004.06.017

post-traumatic stress disorder [24,25]. Furthermore, the hippocampus is one of only a few brain regions where the production of neurons occurs throughout the lifetime of animals, including human [7]. Furthermore, hippocampal neurogenesis is influenced by various environmental factors and stimuli [11,21,29]. For example, both acute and chronic stress cause a decrease in cell proliferation [8].

These findings indicate that cell death, neurogenesis, and the more dramatic changes induced by chronic stress occur in hippocampus together with stress-related disorders. To compare gene expression in the hippocampus in normal and an animal model of mental disorder, we analyzed gene expression in this region of the brain by large-scale sequencing of randomly selected clones from the cDNA library to generate expressed sequence tags (ESTs).

We also illustrate one use of these clone sets by constructing a cDNA microarray focused on genes categorized into 'cell/organism defense'. These nonredundant hippocampus clone sets and our own microarray promise to become a useful tool for molecular studies of animal models of stress-related disorders.

2. Materials and methods

2.1. cDNA sequencing

A non-unidirectional cDNA library with inserts larger than ~400 bp, which was constructed using mRNAs from adult rat hippocampus and Lambda ZAP® II vector system, was purchased from commercial company (Stratagene, La Jolla, CA, USA). Plasmid DNA were prepared as described previously [28]. Briefly, the non-unidirectional cDNA library was excised in vivo from the λ phage into phagemid DNA using the ExAssist® helper phage (Stratagene). Phagemid particles were transfected into *Escherichia coli* SOLR (Stratagene) and plated on LB plates containing ampicillin to generate plasmid forms. The colonies were randomly selected from the plates and plasmid DNAs were extracted using the Biomek 2000 miniprep systems (Beckman, Fullerton, CA, USA). The inserts of the cDNA clones were sequenced from both ends. DNA sequencing was performed using an ABI PRISM BigDye Terminator Cycle Sequencing FS Ready Reaction Kit® (Applied Biosystems, Foster, CA, USA). The sequencing reaction products were analyzed by an Applied Biosystems DNA sequencer model 377. Quality assessment and base trimming of each sequence were performed using PE Sequencing Analysis 3.3 software (Applied Biosystems). Contaminated vector sequences were removed using Assembly LIGN® (copyright by Oxford Molecular Group). Sequences containing less than 1% ambiguous bases longer than 200 bp were counted as good sequences.

2.2. Database analysis of rat hippocampus ESTs

We analyzed ~13,867 ESTs from rat hippocampus with non-redundant nucleotide and peptide sequences extracted in silico from GenBank databases at the National Center for Biotechnology Information (NCBI) (http://www.ncbi.nlm.nih.gov/). We first removed tracks of ambiguous residues from the obtained ESTs and masked the highly repetitive sequences by RepeatMasker (http://ftp.genome.washington.edu/RM/RepeatMasker.html). The resultant sequences were subjected to a BLAST search against a merged database containing daily updates of rat sequences from GenBank. The program BLASTN [2] was used to compare the sequences at the level of the nucleic acids. If a query EST sequence shared more than 95% sequence identity without masked and ambiguous nucleotides and showed a score of more than 365 with any other sequences in the database, it was grouped with the query. If there was at least one sequence in common, groups were merged into a single cluster. An EST sequence that did not belong to any of the clusters is a singleton. To assemble the sequences that belonged in each cluster, we applied the Labo Server® system to make contigs (World Fusion, Tokyo, Japan). The EST clones without any match to known genes in the nucleotide database were retrieved by the BLASTX program [2], which was used to conceptually translate the sequence in all six reading frames and compare the sequences with those in the peptide database at NCBI (http://www.ncbi.nlm.nih.gov/).

Role categories and subcategories were chosen to encompass a broad view of rat cell biology. Although many categorization schemes might be considered equally valid, we have attempted to group together proteins that share similar functional characteristics or cellular roles rather than by a strict biochemical classification. Roles were assigned according to the known or putative involvement of a gene or protein in a cellular process or pathway as opposed to participation in a specific binding or catalysis function on which Gene Ontology (GO) annotations are based.

We used a seventh broad category, unclassified, for proteins and genes of unknown role or which could not be assigned with confidence based on searches of the literature [1]. The EST clones matching known genes (excluding repetitive elements and probable microbial contaminant sequences) were catalogued into seven general categories (cell division, cell signaling/cell communication, cell structure/motility, cell/organism defense, gene/protein expression, metabolism and unclassified) and subcategorized according to specific function based on the putative functions of the known genes using the Genome Directory (http://www.tigr.org/tdb/hgi.html), UniGene, Entrez and PubMed at the NCBI. Two subcategories were included in cell structure/motility, namely, contractile proteins and vesicular transport [1,13].

Table 1
Summary of rat hippocampus ESTs

	Known genes	Unknown genes	Total
Cluster	1282	512	1794
Singleton	1312	4067	5379
Total	2594	4579	7173

2.3. Animals and treatment

Adult Sprague–Dawley rats (Charles River, Yokohama, Japan) were sacrificed by decapitation, and hippocampus were quickly dissected on an ice plate, immediately frozen with liquid nitrogen and stored at −80 °C until RNA isolation. All procedures were performed in accordance with our institutional guidelines after obtaining the permission of the Laboratory Animal Committee of Gunma University.

2.4. Construction of an original cDNA microarray

For future investigation of the genotype of stress responses in the nerve system, 115 clones related in 'cell/organism defense' were selected from the collected ESTs. Clones were amplified by PCR using ExTaq® (TaKaRa Shuzou, Kyoto, Japan) in a 50 μl reaction mixture and PCR was performed 12 times for each clone. Amplification was performed as follows: 3 min at 94 °C for initial denaturation, 35 cycles of 94 °C denaturing for 30 s, 60 °C annealing for 30 s and 72 °C extension for 1 min, followed by a final extension at 72 °C for 10 min. The quality and quantity of purified PCR product was confirmed using 1.2% agarose gel electrophoresis. One hundred and four of 115 clones that gave a single band then were used to construct an original cDNA microarray. Purified PCR products of each clone were resuspended in 3×SSC so that concentrations of nucleotide would be about 1 μg/μl. cDNA solutions were spotted onto poly-L-lysine-coated microarray slides (Matsunami Glass, Japan) using a capillary pen styled arrayer (OmniGrid™). cDNA spotted slides were then exposed to 120 mJ of 254 nm light to crosslink DNA on slides. Lambda phage DNA were spotted as negative controls, and GAPDH and 18S rRNA were used as positive controls.

Table 2
Redundancy of nucleotide sequences from the cDNA clones

Redundancy	No. of groups	Percentage
1	5379	75.0
2	953	13.3
3	348	4.9
4	165	2.3
5	85	1.2
6–10	158	2.2
11–20	62	0.9
21–50	22	0.3
51–100	0	0.0
>100	2	0.0

2.5. Hybridization and analysis

Total RNA was extracted from hippocampus using Qiagen RNeasy RNA extraction Kit (Qiagen, Valencia, CA, USA). We confirmed extraction of a high yield of intact total RNA by 1.2% formaldehyde agarose gel. The cDNA probes were generated by RNA reverse transcription under BD PowerScript Reverse Transcriptase (Clontech, Palo Alto, CA, USA) with a modified oligo (dT) primer (the BD SMART CDS Primer IIA, Clontech). cDNA probes then were labeled with a modified indirect labeling protocol using BD Atlas SMART Fluorescent Probe Amplification Kit® (Clontech). Briefly, primary aliphatic amino groups are incorporated through primer extension using a dNTP mix, which includes the dTTP analog, aminoallyl-dUTP. The aminoallyl-dUTP-labeled cDNA probes then are labeled with Cy3 dye (Amersham Biosciences, Piscataway, NJ, USA). In preparation for hybridization, the cDNA pellets were resuspended in 25 μl sterile deionized water. The probes then were mixed with 20 μg poly dA, 20 μg tRNA and 20 μg mouse Cot1 DNA, and finally resuspended in 50 μl of 3.4×SSC/0.5% SDS. The probe was incubated at 95 °C for 5 min, transferred to a prehybridized glass array and incubated for 18 h in a hybridization chamber (KakenGeneqs, Chiba, Japan) at 65 °C. After the hybridization, glass arrays were washed three times with agitation in the following solutions: 2×SSC/0.1% SDS for 2 min, 1×SSC/0.1% SDS for 2 min and 0.2×SSC/0.1% SDS for 2 min at room temperature. Arrays then were dried by centrifugation in a slide rack for 2 min at 800 rpm. All slides were scanned immediately using a ScanArray®Lite (PerkinElmer, Boston, MA, USA). Image analysis was performed with QuantArray (PerkinElmer) and background intensities were determined by the median pixel values.

3. Results

3.1. Characterization of rat hippocampus ESTs

A total of ~15,000 random clones from a non-unidirectional cDNA library were partially sequenced from the 3′- and 5′-end to generate 13,660 sequences with good quality. Such large-scale sequencing generally provides highly redundant ESTs that can be aligned and assembled for a set of unique genes. After 985 repetitive (7.1%) sequences and 323 mitochondrial (2.3%) DNAs were removed, the remaining ESTs were assembled into non-redundant sequence groups. The clustering analysis generated 7173 non-redundant sequences comprising 1794 groups of sequences and 5379 singletons (Table 1). Of these, 2594 were known genes. Relative frequencies of the ESTs for each gene reflect the average level of expression of the corresponding mRNAs in the pooled tissues. Since groups with redundancy of 1–5 times accounted for 96.6% of the groups, our massive sequencing was clearly effective in

Table 3
List of highly redundant cDNA clones

Redundancy	Gene products	Cellular function
119	myelin basic protein	cell structure/motility
111	proteolipid protein	cell structure/motility
50	synaptic vesicle glycoprotein 2 b	vesicular transport
47	hydroxy-δ-5-steroid dehydrogenase, 3β- and steroid δ-isomerase 1	lipid
44	myelin-associated oligodendrocytic basic protein	cell structure/motility
42	polyubiquitin	posttranslation modification/targeting
39	SNAP25 interacting protein	vesicular transport
38	calmodulin 1	effectors/modulators
35	glial fibrillary acidic protein	cytoskeletal
35	heat shock protein 8	stress response
34	eukaryotic translation elongation factor 1α1	translation factors
33	β-spectrin 3	cytoskeletal
32	calcium/calmodulin-dependent protein kinase IIα subunit	protein modification
32	SPARC-like 1	extracellular matrix
28	kinesin family member 5C	microtubule-associated proteins/motors
27	amyloidogenic glycoprotein (rAG), cognate of human A4 amyloid precursor protein	cell adhesion
26	development-related protein	unclassified
26	glutamine synthetase 1	amino acid
24	ATPase, Na^+K^+ transporting, α2	transport
24	heat shock protein 1, α	stress response
23	microtubule-associated protein 2	microtubule-associated proteins/motors
22	ATPase Na^+/K^+ transporting β1 polypeptide	transport
21	heat shock protein 90	stress response
21	stearoyl-coenzyme A desaturase 2	lipid
19	calmodulin 3	effectors/modulators
19	ribonucleotide reductase M2 subunit	nucleotide
18	myelin and lymphocyte protein	unclassified
18	neurochondrin	unclassified
18	reticulon 3	unclassified
18	syntaxin binding protein 1	vesicular transport
17	α-spectrin 2	cytoskeletal
17	cadherin 22	cell adhesion
17	glutamate oxaloacetate transaminase 1	amino acid
17	*Rattus norvegicus* clone RP31-464J4 strain Brown Norway	unclassified
17	tyrosine 3-monooxygenase/ tryptophan 5-monooxygenase activation protein, ζ polypeptide	protein modification
16	aldolase C, fructose-biphosphate	sugar/glycolysis
16	α-tubulin	cytoskeletal
16	glutamate receptor, ionotropic, 2	receptors
16	prion protein	transcription factors
16	protein carrying the RING-H2 sequence motif	posttranslation modification/targeting
16	protein tyrosine phosphatase, receptor type, D	receptors
15	adaptor-related protein complex 2, μ1 subunit	vesicular transport
15	carboxypeptidase E	protein turnover
15	dynamin 1	cytoskeletal
15	neural visinin-like Ca^{2+}-binding protein type 2	effectors/modulators
15	neuronal pentraxin receptor	receptors
15	solute carrier family 1, member 3	channels/transport
14	ATPase, H^+ transporting, lysosomal (vacuolar proton pump), β 56/58 kDa, isoform 2	transport
14	chimerin (chimaerin) 1	intracellular transducers
14	DEAD (Asp–Glu–Ala–Asp) box polypeptide 5	RNA processing
14	myelin-associated glycoprotein	cell structure/motility
14	*N*-ethylmaleimide sensitive factor	carrier proteins/ membrane transport
14	prosaposin	unclassified
14	triosephosphate isomerase 1	sugar/glycolysis
13	growth arrest specific 7	cell cycle
13	protein tyrosine kinase 2β	protein modification
13	SNRPN upstream reading frame	unclassified
13	system N1 Na^+ and H^+-coupled glutamine transporter	channels/transport
13	tumor differentially expressed 1	unclassified
12	ankyrin 3 (G)	cytoskeletal
12	brain Ntab mRNA sequence	unclassified
12	C1-13 gene product	unclassified
12	eukaryotic translation elongation factor 2	translation factors
12	hippocalcin	effectors/modulators
12	nasal embryonic LHRH factor	unclassified
12	*Rattus norvegicus* clone RP31-422M21 strain Brown Norway	unclassified
12	S100 protein, β polypeptide	effectors/modulators
12	similar to RIKEN cDNA 1700001E04	unclassified
12	synaptotagmin 1	effectors/modulators
12	tyrosine 3-monooxygenase/ tryptophan 5-monooxygenase activation protein, γ polypeptide	protein modification
12	v-raf-1 murine leukemia viral oncogene homolog 1	cell division
11	adaptor-related protein complex 3, β2 subunit	vesicular transport
11	amyloid β (A4) precursor-like protein 1	protein turnover
11	ATPase, Na^+K^+ transporting, α3 subunit	transport
11	C1q-like	unclassified
11	cytoplasmic FMR1 interacting protein 2	unclassified
11	diacylglycerol kinase ζ	lipid
11	glycoprotein m6b	cell structure/motility

(continued on next page)

Table 3 (*continued*)

Redundancy	Gene products	Cellular function
11	inositol 1,4,5-triphosphate receptor 1	receptors
11	mitogen-activated protein kinase 8 interacting protein 3	protein modification
11	nel-like 2 homolog (chicken)	unclassified
11	neurexin 1	cell adhesion
11	nucleolar protein 3 (apoptosis repressor with CARD domain)	unclassified
11	similar to expressed sequence C85658	unclassified
11	thymus cell antigen 1, θ	immunology
11	tyrosine 3-monooxygenase/ tryptophan 5-monooxygenase activation protein, θ polypeptide	protein modification
10	adenomatosis polyposis coli	cell division
10	synaptosomal-associated protein	cell division
10	ATP/GTP binding protein 1	intracellular transducers
10	cyclic nucleotide phosphodiesterase 1	metabolism
10	nuerabin 2	cytoskeletal
10	neurofilament 3, medium	cytoskeletal
10	dystonin	extracellular matrix
10	limbic system-associated membrane protein	immunology
10	bruno-like 4, RNA binding protein (Drosophila)	RNA processing
10	tripartite motif protein 3	transcription factors
10	similar to ORF2 consensus sequence encoding endonuclease and reverse transcriptase minus RNascH	transcription factors
10	protein phosphatase 2a, catalytic subunit, α isoform	protein modification
10	phosphofructokinase, platelet	sugar/glycolysis
10	Nogo-A	unclassified
10	sperm membrane protein (YWK-II)	unclassified

identifying a larger number of non-redundant mRNAs expressed at moderate levels (Table 2). Approximately 2.2% of the ESTs were identified 6–10 times. One hundred and one abundant sequences identified more than nine times (1.4%) are shown in Table 3. Of these, myelin basic protein (118 times) and brain myelin proteolipid protein (PLP) (111 times), the major extrinsic myelin protein and the major integral myelin membrane protein, respectively, are most abundant in this library.

3.2. Expression profile of known genes in rat hippocampus

The ESTs showing identity or high similarity to known genes were classified into seven major categories on the basis of putative general functions of the protein encoded, as described previously (categories; 'cell division', 'cell signaling/communication', 'cell structure/motility', 'cell/organism defense', 'gene/protein expression', 'metabolism' and 'unclassified') [1,13]. In total, 2594 known genes are represented in the classified data set (supplement at http://imcr.showa.gunma-u.ac.jp/lab/genetics/RHippocampus.zip). In concordance with the results in ESTs from brain observed by Adams et al., the largest category of genes was 'cell signaling and communication' except for the category 'unclassified' (618 genes, 23.8%) (Fig. 1). Successively smaller categories were 'gene/protein expression' (19.1%), 'metabolism' (13.8%), 'cell structure/motility' (9.5%), 'cell division' (4.8%) and 'cell/organism defense' (4.4%). ESTs lacking sufficient information to be classified constituted the remainder (24.5%). To further analyze the molecular complexity, each major category was subdivided according to the putative specific functions of the proteins (supplement at http://imcr.showa.gunma-u.ac.jp/lab/genetics/RHippocampus.zip). For example, the largest category, 'cell signaling and communication', was subdivided into eight subgroups (Fig. 2). Of these, 'protein modification' includes the largest number of non-redundant genes (145 genes) and ESTs for that function are also identified most frequently (429 ESTs for 145 different proteins).

3.3. Rat homologs of known genes and new members of gene families

In this study, 63.8% of the non-redundant ESTs did not match any of the known genes in the nucleotide database. To identify novel rat genes encoding proteins structurally related to the known proteins, we performed BLASTX search in the peptide databases using 4579 ESTs, with *P*-value of 10^{-10} and score of 60 as the cut off for significant similarity. Five hundred and ninety-nine non-redundant ESTs match this condition and, of these, 169 ESTs represent rat homologs of genes identified in mouse or new members of structurally related families in rat (Table 4). Of these, the proteins similar to NEDD-4 protein, retrovirus-related POL polyproteins and zinc finger proteins were most abundant. Functional analyses of the proteins identified through this approach should clarify the role of new members of structurally related families in hippocampus. The remaining ESTs (3980 genes) were not related to any other sequences in the databases. As found in similar large-scale cDNA sequencing studies carried out in other tissues, about 50% of the clones appear to be derived from genes that have not previously been described.

3.4. Construction of an original cDNA microarray

In this study, we illustrate one use of these clone sets by constructing a cDNA microarray focused on genes categorized into 'cell/organism defense' for use in further molecular studies of animal models of stress-related disorders. The hybridization pattern of normal adult rat hippocampal cDNA by our own microarray is shown in Fig. 3A and B. The 104 clones, 2 positive and 1 negative controls are spotted on the glass 10 times each. (Table 5). A

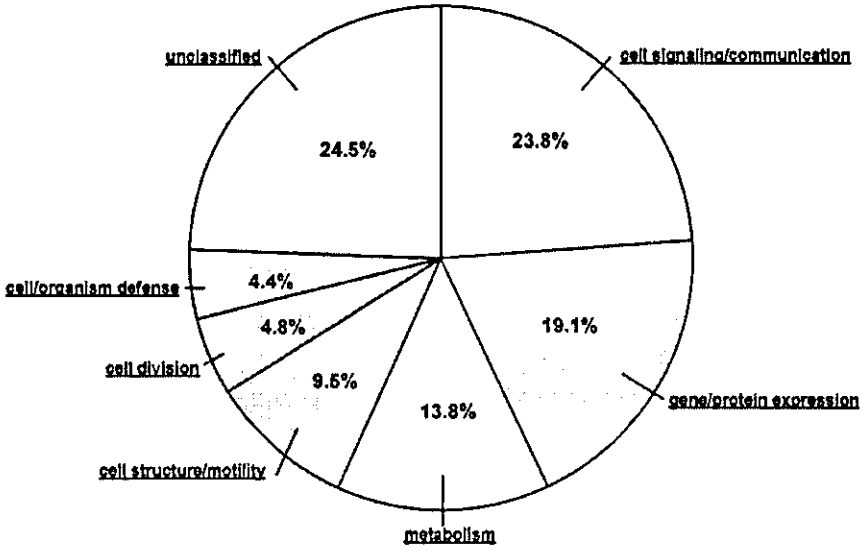

Fig. 1. Functional distribution of known genes in rat hippocampus. ESTs showing identity or high similarity to known genes were classified into seven major categories on the basis of the putative general functions of the protein encoded.

number of heat shock proteins (HSPs) and stress inducible proteins are certainly expressed also in normal rat hippocampus. As shown in Fig. 3 C, there was significant correlation between the frequencies of observed ESTs and the signal intensities of the spots (r=0.713).

4. Discussion

Expression profiling using serial analysis of gene expression (SAGE) tags and ESTs is a potent method for identifying and characterizing both known and novel genes in a given tissue. Over the past few years, cDNA libraries have been prepared from many tissues and cell lines, from which a large number of SAGE tags and ESTs have been studied. An expression profile of 30,000 genes in rat hippocampus using the SAGE method has been reported previously [5]. While SAGE analysis is unique in its ability to quantify gene expression in a given tissue with extremely high throughput, there are several limitations for the analysis of the data. For example, SAGE generates tags from the most 3′ -*Nla*III restriction site, but only on those mRNAs that have the site. Therefore, SAGE may under-perform because specific transcripts may be missed due to the absence of a recognition site for the anchoring enzyme or GC-content bias [17]. In addition, tag to gene

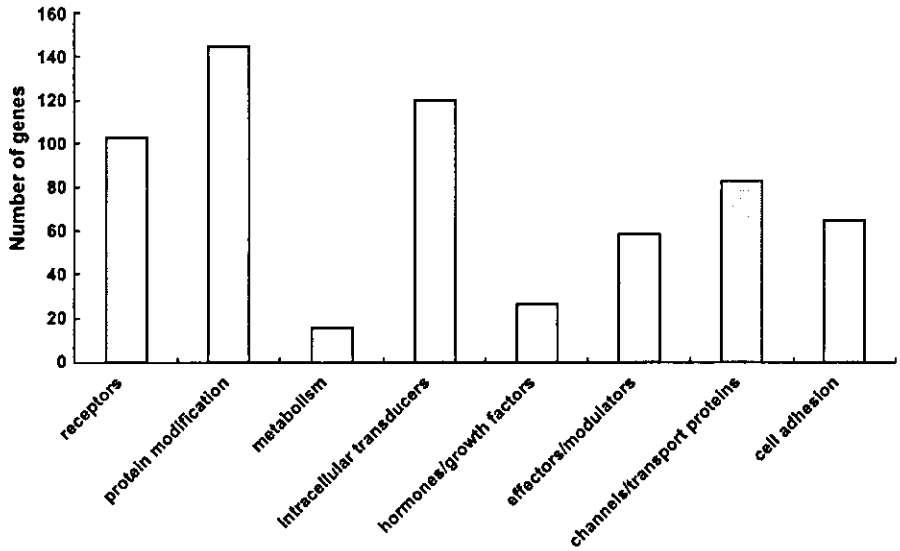

Fig. 2. Subclasses of the cell signaling/communication category. The largest category in Fig. 1 was subdivided into eight subgroups. Of these, the protein modification subgroup contains the largest number of non-redundant genes.

Table 4
Homologs of known genes and new members of gene families

Gene name	Species	Score	*P*-value	No.
14-3-3 protein eta	*Mus musculus*	85	4.00E−17	1
60S ribosomal protein L10	*Mus musculus*	58	1.00E−08	1
60S ribosomal protein L14	*Rattus norvegicus*	88	7.00E−26	1
60S ribosomal protein L34	*Mus musculus*	106	3.00E−23	1
Acetyl-CoA acetyltransferase, mitochondrial precursor	*Rattus norvegicus*	73	3.00E−13	1
Acyl-coenzyme A oxidase 1, peroxisomal	*Rattus norvegicus*	104	4.00E−23	1
AF-10 protein	*Mus musculus*	125	4.00E−29	1
Alcohol dehydrogenase class III	*Rattus norvegicus*	219	2.00E−60	1
α-Actinin 3	*Mus musculus*	199	3.00E−51	1
Amine oxidase	*Rattus norvegicus*	78	3.00E−15	1
Amyloid-like protein 1 precursor	*Mus musculus*	150	5.00E−37	1
Armadillo repeat protein deleted in velo-cardio-facial syndrome homolog	*Mus musculus*	116	3.00E−26	1
Armadillo repeat protein deleted in velo-cardio-facial syndrome homolog	*Mus musculus*	114	1.00E−25	1
Armadillo repeat protein deleted in velo-cardio-facial syndrome homolog	*Mus musculus*	51	7.00E−07	1
ATP synthase A chain	*Mus musculus*	56	1.00E−08	1
ATP-dependent DNA helicase II, 70-kDa subunit	*Mus musculus*	70	2.00E−12	1
Basement membrane-specific heparan sulfate proteoglycan core protein precursor	*Mus musculus*	87	1.00E−17	1
BCL2/adenovirus E1B 19-kDa protein-interacting protein 2	*Mus musculus*	134	6.00E−32	1
β-Chimerin	*Rattus norvegicus*	109	3.00E−24	1
β-Secretase precursor	*Rattus norvegicus*	99	6.00E−21	1
BRCA1-associated RING domain protein 1	*Rattus norvegicus*	77	2.00E−14	1
C-Rel proto-oncogene protein	*Mus musculus*	138	9.00E−38	1
Calcium-binding mitochondrial carrier protein Aralar2	*Mus musculus*	67	9.00E−12	1
cAMP-dependent protein kinase type I-β regulatory chain	*Rattus norvegicus*	130	2.00E−30	3
cAMP-dependent protein kinase type II-α regulatory chain	*Rattus norvegicus*	58	3.00E−17	2
Carbonic anhydrase XIV precursor	*Mus musculus*	57	2.00E−08	1
Carboxypeptidase H precursor	*Rattus norvegicus*	173	2.00E−43	1
Cathepsin B precursor	*Rattus norvegicus*	97	6.00E−21	1
Chloride channel protein 6	*Mus musculus*	260	9.00E−70	1
Chromobox protein homolog 6	*Mus musculus*	192	4.00E−50	1
Cofilin, muscle isoform	*Mus musculus*	52	2.00E−07	2
Cyclic-AMP-dependent transcription factor ATF-5	*Mus musculus*	69	5.00E−12	1
Cytochrome *B*	*Rattus norvegicus*	70	2.00E−12	1
Cytochrome *c* oxidase polypeptide II	*Mus musculus*	104	7.00E−23	1
Cytohesin 2	*Mus musculus*	64	2.00E−10	1
Density-regulated protein	*Mus musculus*	115	6.00E−26	1
Destrin	*Mus musculus*	145	2.00E−35	1
Developmentally regulated GTP-binding protein 1	*Mus musculus*	150	9.00E−37	1
DGCR6 protein	*Mus musculus*	84	6.00E−17	1
Disks large-associated protein 1	*Rattus norvegicus*	103	6.00E−23	1
DNA binding protein URE-B1	*Rattus norvegicus*	79	5.00E−15	1
DNA-binding protein SATB1	*Mus musculus*	62	4.00E−10	1
DnaJ homolog subfamily C member 4	*Mus musculus*	85	2.00E−17	1
Dual specificity protein phosphatase 8	*Mus musculus*	161	5.00E−40	1
Ectoderm-neural cortex-1 protein	*Mus musculus*	68	5.00E−16	1
Ectoderm-neural cortex-1 protein	*Mus musculus*	83	2.00E−16	1
Ectonucleotide pyrophosphatase/ phosphodiesterase 1	*Mus musculus*	55	8.00E−08	2
Elongation factor 2	*Rattus norvegicus*	99	5.00E−21	1
Enhancer of zeste homolog 1	*Mus musculus*	62	6.00E−10	1
Exostosin-1	*Mus musculus*	104	6.00E−23	1
FK506-binding protein precursor	*Mus musculus*	67	2.00E−11	1
Focal adhesion kinase 1	*Rattus norvegicus*	102	1.00E−22	1
Galactocerebrosidase precursor	*Mus musculus*	90	7.00E−19	1

Table 4 (*continued*)

Gene name	Species	Score	*P*-value	No.
Glucose-6-phosphate isomerase	*Mus musculus*	159	3.00E−39	1
Glutamate receptor 1 precursor	*Mus musculus*	116	3.00E−26	2
Glutamate receptor, ionotropic kainate 5 precursor	*Rattus norvegicus*	56	2.00E−08	1
Guanine nucleotide exchange factor DBS	*Rattus norvegicus*	89	5.00E−18	1
Guanine nucleotide releasing protein (GNRP) (P140 Ras-GRF)	*Rattus norvegicus*	100	7.00E−22	1
Guanine nucleotide-binding protein β subunit 5	*Mus musculus*	79	2.00E−15	3
Guanine nucleotide-binding protein G(q), α subunit	*Rattus norvegicus*	59	2.00E−09	2
Guanine nucleotide-binding protein G(S), α subunit	*Mus musculus*	99	1.00E−21	1
Histidine-rich membrane protein Ke4	*Mus musculus*	85	4.00E−17	1
Histone deacetylase 6	*Mus musculus*	188	4.00E−48	2
Importin α-3 subunit	*Mus musculus*	78	5.00E−15	1
Inhibitor of nuclear factor κ-B kinase α subunit	*Mus musculus*	85	9.00E−28	1
Integral membrane protein 2B	*Mus musculus*	74	1.00E−13	1
Integrin α-6 precursor	*Mus musculus*	72	9.00E−13	2
Inter-α-trypsin inhibitor heavy chain H3 precursor	*Rattus norvegicus*	102	4.00E−22	1
Interferon-α/β receptor α chain precursor	*Mus musculus*	65	3.00E−11	1
Kinesin-like protein KIF3A	*Mus musculus*	74	1.00E−13	1
Lamin B3	*Mus musculus*	125	7.00E−29	1
Latent transforming growth factor β binding protein 1 precursor	*Rattus norvegicus*	95	9.00E−20	1
Leukocyte tyrosine kinase receptor precursor	*Mus musculus*	78	9.00E−15	1
LIM/homeobox protein Lhx6.1	*Mus musculus*	80	1.00E−15	1
Low molecular weight phosphotyrosine protein phosphatase ACP1/ACP2	*Rattus norvegicus*	97	2.00E−20	1
Lysosomal α-mannosidase precursor	*Mus musculus*	136	2.00E−32	1
Lysosomal α-mannosidase precursor	*Mus musculus*	110	1.00E−32	1

Table 4 (*continued*)

Gene name	Species	Score	*P*-value	No.
Methionyl-tRNA formyltransferase, mitochondrial precursor	*Mus musculus*	87	2.00E−17	1
Methylmalonate-semialdehyde dehydrogenase [acylating], mitochondrial precursor	*Rattus norvegicus*	84	1.00E−16	1
Microtubule-associated protein 1A	*Mus musculus*	73	1.00E−13	1
Microtubule-associated protein 4	*Mus musculus*	95	6.00E−20	2
Mitochondrial trifunctional enzyme α subunit precursor	*Rattus norvegicus*	112	3.00E−25	1
Mitogen-activated protein kinase 7	*Mus musculus*	125	4.00E−29	1
Myelin and lymphocyte protein	*Rattus norvegicus*	58	1.00E−08	1
Myelin basic protein S	*Rattus norvegicus*	90	2.00E−18	1
Myotubularin-related protein 3	*Mus musculus*	50	4.00E−07	1
NADPH/adrenodoxin oxidoreductase, mitochondrial precursor	*Rattus norvegicus*	72	5.00E−13	1
NEDD-4 protein	*Mus musculus*	56	3.00E−08	1
NEDD-4 protein	*Mus musculus*	54	1.00E−07	1
NEDD-4 protein	*Mus musculus*	54	1.00E−07	1
NEDD-4 protein	*Mus musculus*	54	1.00E−07	1
NEDD-4 protein	*Mus musculus*	53	4.00E−07	1
NEDD-4 protein	*Mus musculus*	53	2.00E−07	1
NEDD-4 protein	*Mus musculus*	51	8.00E−07	1
NEDD-4 protein	*Mus musculus*	56	4.00E−08	1
NEDD-4 protein	*Mus musculus*	54	5.00E−08	1
NEDD-4 protein	*Mus musculus*	53	1.00E−07	1
Neighbor of A-kinase anchoring protein 95	*Mus musculus*	88	1.00E−17	1
Neural Wiskott-Aldrich syndrome protein	*Rattus norvegicus*	125	1.00E−29	1
Neuroendocrine convertase 3 precursor	*Mus musculus*	70	3.00E−12	2
Neuronal membrane glycoprotein M6-A	*Mus musculus*	56	1.00E−08	2
Neuronal-specific septin 3	*Mus musculus*	55	1.00E−07	3
NGFI-A binding protein 1	*Rattus norvegicus*	92	7.00E−19	1
Nidogen-2 precursor	*Mus musculus*	50	2.00E−12	2
NK-tumor recognition protein	*Mus musculus*	120	2.00E−27	1
Nucleolin	*Rattus norvegicus*	57	8.00E−09	2
Numb-like protein	*Mus musculus*	213	2.00E−55	1
Peroxisomal targeting signal 2 receptor	*Mus musculus*	59	7.00E−09	1

(continued on next page)

Table 4 (*continued*)

Gene name	Species	Score	*P*-value	No.
Phosphatidylinositol-glycan-specific phospholipase D1 precursor	*Mus musculus*	127	1.00E−29	1
Phospholipase D2	*Rattus norvegicus*	58	1.00E−08	1
Phospholipid hydroperoxide glutathione peroxidase, mitochondrial precursor	*Rattus norvegicus*	114	6.00E−26	1
Polyadenylate-binding protein 1	*Mus musculus*	61	3.00E−10	1
Potential phospholipid-transporting ATPase IIA	*Mus musculus*	54	4.00E−08	1
Pristanoyl-CoA oxidase	*Rattus norvegicus*	82	2.00E−16	1
Probable calcium-binding protein Dd112	*Mus musculus*	58	1.00E−08	1
Probable cation-transporting ATPase 1	*Mus musculus*	130	4.00E−31	1
Prostaglandin F2-α receptor regulatory protein precursor	*Rattus norvegicus*	74	2.00E−13	1
Protein kinase C, γ type	*Mus musculus*	129	5.00E−30	1
Proto-oncogene tyrosine-protein kinase MER precursor	*Rattus norvegicus*	68	1.00E−11	1
Protocadherin 3 precursor	*Rattus norvegicus*	120	9.00E−28	1
Putative protein C21orf62 homolog	*Mus musculus*	185	6.00E−47	3
Ras-related protein Rab-1B	*Rattus norvegicus*	113	1.00E−25	1
Regulator of G-protein signaling 5	*Rattus norvegicus*	97	9.00E−21	1
Retrovirus-related POL polyprotein	*Mus musculus*	146	1.00E−35	1
Retrovirus-related POL polyprotein	*Mus musculus*	52	4.00E−07	1
Retrovirus-related POL polyprotein	*Mus musculus*	134	1.00E−31	1
Retrovirus-related POL polyprotein	*Mus musculus*	94	2.00E−19	1
Retrovirus-related POL polyprotein	*Mus musculus*	75	3.00E−14	1
Retrovirus-related POL polyprotein	*Mus musculus*	65	7.00E−11	1
Retrovirus-related POL polyprotein	*Mus musculus*	60	2.00E−09	1
Retrovirus-related POL polyprotein	*Mus musculus*	59	3.00E−15	2
Retrovirus-related POL polyprotein	*Mus musculus*	56	5.00E−08	1
RING finger protein 27	*Mus musculus*	147	9.00E−36	2
RING finger protein 4	*Rattus norvegicus*	65	3.00E−11	1

Table 4 (*continued*)

Gene name	Species	Score	*P*-value	No.
Semaphorin 4D precursor	*Mus musculus*	91	2.00E−18	1
Semaphorin 5A precursor	*Mus musculus*	121	2.00E−28	1
Semaphorin 6B precursor	*Rattus norvegicus*	61	2.00E−09	1
Septin 2	*Mus musculus*	87	3.00E−17	1
Serine/threonine protein kinase 25	*Mus musculus*	70	9.00E−13	7
Serine/threonine-protein kinase 19	*Mus musculus*	114	9.00E−26	1
Single-minded homolog 2	*Mus musculus*	68	9.00E−12	1
Sodium/calcium exchanger 2 precursor	*Rattus norvegicus*	73	1.00E−13	1
SOX-13 protein	*Mus musculus*	149	2.00E−36	1
Splicing factor 3B subunit 1	*Mus musculus*	123	7.00E−29	1
SSXT protein	*Mus musculus*	71	7.00E−13	1
Surfeit locus protein 6	*Mus musculus*	58	2.00E−10	1
Synaptojanin 2	*Rattus norvegicus*	70	4.00E−12	1
T-cell receptor α chain V region 2B4 precursor	*Mus musculus*	80	3.00E−15	3
T-complex protein 1, δ subunit	*Mus musculus*	53	2.00E−07	1
TLM protein	*Mus musculus*	62	8.00E−10	5
Transcription factor 17	*Mus musculus*	86	7.00E−17	1
Ubiquinol-cytochrome *C* reductase complex core protein I, mitochondrial precursor	*Mus musculus*	205	5.00E−53	1
Ubiquitin carboxyl-terminal hydrolase 2	*Mus musculus*	127	3.00E−30	2
Uridine kinase	*Mus musculus*	127	7.00E−30	1
Voltage-gated potassium channel protein Kv3.1	*Mus musculus*	109	1.00E−24	1
VPS26 protein homolog	*Mus musculus*	134	1.00E−31	1
VPS26 protein homolog	*Mus musculus*	74	5.00E−14	1
Werner syndrome helicase homolog	*Mus musculus*	159	3.00E−39	1
X inactive specific transcript protein	*Mus musculus*	49	5.00E−07	1
Zinc finger homeobox protein 1b	*Mus musculus*	137	3.00E−33	1
Zinc finger protein 27	*Mus musculus*	57	1.00E−08	1
Zinc finger protein 37	*Mus musculus*	86	3.00E−17	1
Zinc finger protein 37	*Mus musculus*	77	1.00E−14	1
Zinc finger protein 46	*Mus musculus*	135	2.00E−32	1
Zinc finger protein 60	*Mus musculus*	136	2.00E−32	1
Zinc finger protein 90	*Mus musculus*	94	2.00E−19	1
Zinc finger protein 92	*Mus musculus*	219	3.00E−59	1
Zinc-finger protein RFP	*Mus musculus*	84	1.00E−16	1

mapping is not completely definitive, as some tags correspond to several genes. Furthermore, incorrect tag counts can arise from incomplete digestion or alternative

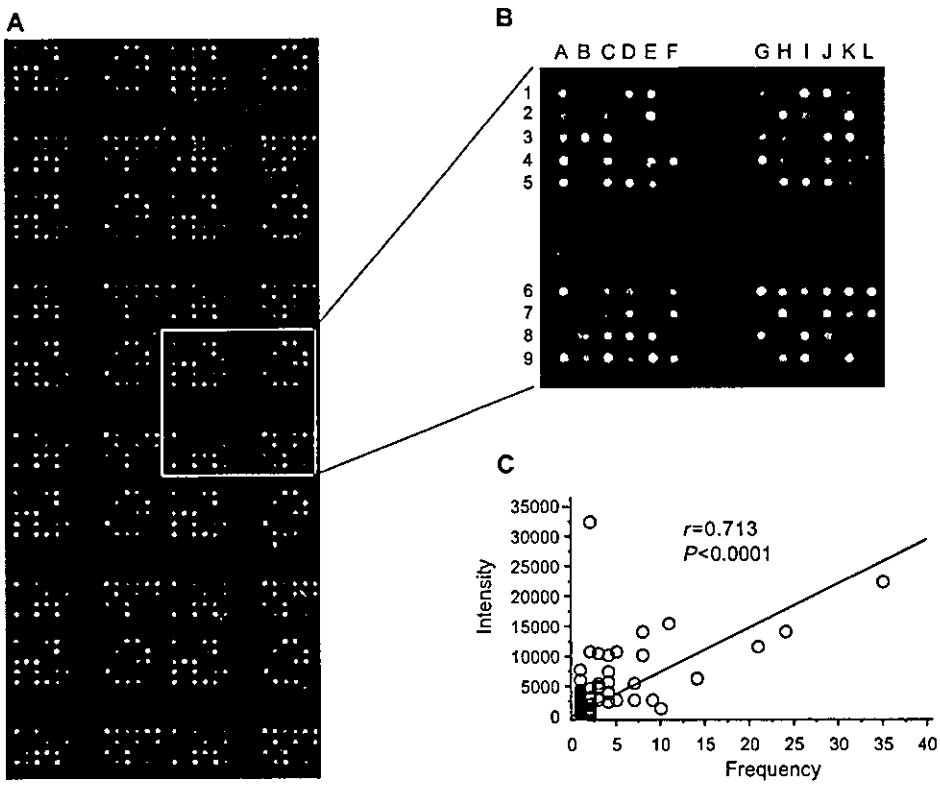

Fig. 3. (A) Hybridization pattern of normal adult rat hippocampal cDNA. The 104 EST clones, 2 positive and 1 negative controls are spotted on the glass 10 times each. (B) Zoom up figure of one sub-array. There are 107 spots in each sub-array. (C) The correlation between the frequencies of observed ESTs and the signal intensities of the spots. There is significant correlation between the frequencies and the signal intensities of the ESTs (r=0.713).

polyadenylation, giving rise to multiple tags derived from a single transcript.

However, there has been no report of large-scale generation of ESTs from rat hippocampus. EST analysis has certain advantages over other methods such as SAGE for examining the transcript repertoire of tissues. In particular, EST sequences that cover regions of the coding sequence can reveal variant transcripts and splice forms, many of which have functional significance.

In this study, we describe a collection of 13,660 hippocampus-related ESTs representing 7173 different transcripts. With respect to overall EST distribution (i.e. known gene matches), the results in rat hippocampus in this study differ somewhat from those obtained from other tissues. The largest category of function has been reported to be gene/protein expression in studies of ESTs in tissues other than brain [1,13,15]. The largest number of genes obtained from the rat hippocampus cDNA library encoded proteins related to 'cell signaling and communication', as in earlier EST study of brain [1]. The functional categorization of known genes reflects general differences in gene expression between different tissues, and may reflect tissue-specific function. For example, calmodulin and CAMK II, genes involved in 'protein modification' of 'cell signaling/communication' were identified most frequently in this research, and play an important role in the early stages of LTP (Long-term potentiation) in hippocampus [9,19,26]. Genes of mitogen-activated protein kinase signaling that belong to the core signaling pathways involved in memory storage [16,18,27] also were found frequently. Tyrosine 3-monooxgenase/tryptophan 5-monooxgenase activation proteins were found in this library abundantly, and play a role in the regulation of serotonin and biosynthesis of brain noradrenaline, reuptake of which is inhibited by antidepressant drugs [14]. In this study, there was also a larger portion of unclassified genes in hippocampus (24.5%) due, at least in part, to the large numbers of hypothetical proteins generated by recent high throughput genome sequencing efforts.

Although the rat genome project has been released [10], a significant fraction of the genes are hypothetical, revealed only by a computer prediction program. Thus, hippocampal transcripts provide a richer resource for analysis of novel genes related to known proteins. This catalog of expressed genes should facilitate the development of tissue-specific cDNA microarray technology.

Various kinds of stress induce the synthesis of stress proteins that protect cells from subsequent lethal stress. HSPs are ubiquitous cellular proteins with a highly conserved structure, mode of regulation, and function, indicating their important role in cellular functions. HSPs are induced by physical and chemical insults, and confer

Table 5
Gene list of microarray

Spot	Gene name
A1	β prime COP
A2	adenylate kinase 1
A3	HLA-B-associated transcript 1A
A4	heat shock protein 90 (rats, brain, mRNA, 2524 nt)
A5	calnexin
A6	branched chain aminotransferase 1, cytosolic
A7	P450 (cytochrome) oxidoreductase
A8	X-ray repair cross-complementing group 1 protein
A9	carbonic anhydrase 2
B1	oxygen-regulated protein
B2	neogenin
B3	transferrin
B4	RPT protein similar to yeast MRS2
B5	adenylate kinase 4
B6	nuclear factor of κ light polypeptide gene enhancer in B cells inhibitor-like 1
B7	branched chain aminotransferase 2, mitochondrial
B8	metallothionein 1, pseudogene A
B9	RT1 class Ib gene, H2-TL-like, grc region (N1)
C1	glutathione *S*-transferase omega 1
C2	carbonic anhydrase 11
C3	thymus cell antigen 1, θ
C4	coatomer protein complex, subunit γ1
C5	heat shock protein 60 (liver)
C6	tweety homolog 1 (Drosophila)
C7	excision repair cross-complementing rodent repair deficiency, complementation group 1
C8	calcium binding atopy-related autoantigen 1
C9	heat shock protein 8
D1	hemoglobin, α1
D2	odd Oz/ten-m homolog 4 (Drosophila)
D3	DnaJ (Hsp40) homolog, subfamily B, member 5
D4	endoplasmic reticulum protein 29
D5	Nsf: *N*-ethylmaleimide sensitive factor
D6	esterase 10
D7	acyl-coA oxidase
D8	coatomer protein complex, subunit γ2
D9	surfeit 1
E1	DnaJ-like protein
E2	glutathione *S*-transferase, μ type 3 (Yb3)
E3	activated leukocyte cell adhesion molecule
E4	α thalassemia/mental retardation syndrome X-linked homolog (human)
E5	GAPDH
E6	cleft lip and palate associated transmembrane protein 1
E7	heat shock 70 kDa protein 4
E8	heat shock 70 kDa protein 5
E9	peroxiredoxin 2
F1	cytochrome P450-like protein
F2	topoisomerase (DNA) III β
F3	thioredoxin domain containing 5
F4	superoxide dismutase 2
F5	negative control
F6	complement component factor h
F7	adenylate kinase 5
F8	similar to MHC class Ib RT1.S3
F9	limbic system-associated membrane protein
G1	epoxide hydrolase 1
G2	TAP binding protein
G3	Transthyretin (prealbumin, amyloidosis type I)
G4	hemoglobin β chain complex
G5	MHC class II-associated invariant chain
G6	glutathione *S*-transferase, μ1
G7	DnaJ (Hsp40) homolog, subfamily B, member 1
G8	cytochrome P450, subfamily 51
G9	immunoglobulin superfamily, member 8
H1	ferritin light chain 2
H2	glutathione transferase subunit 8
H3	mannose-binding protein associated serine protease-1
H4	NY-REN-18 antigen
H5	DnaJ (Hsp40) homolog, subfamily B, member 6
H6	T cell receptor γ locus, TCR γ1 and γ3 gene clusters
H7	coatomer protein complex, subunit β1
H8	glutamate cysteine ligase, modifier subunit
H9	Sacm21/RT1-A intergenic region, haplotype RT1n and partial RT1-A gene for MHC class I antigen
I1	heat shock protein 1, α
I2	RAD50 homolog (*S. cerevisiae*)
I3	germline MHC class I gene, complete cds
I4	acyl-coenzyme A oxidase 3, pristanoyl
I5	β-2-microglobulin
I6	DnaJ (Hsp40) homolog, subfamily C, member 5
I7	non MHC restricted killing associated
I8	suppression of tumorigenicity 13 (colon carcinoma) Hsp70-interacting protein
I9	ferritin, heavy polypeptide 1
J1	creatine kinase, brain
J2	HLA-B-associated transcript 3
J3	thioredoxin-like 2
J4	B-cell receptor-associated protein 37
J5	selenium-dependent glutathione peroxidase mRNA, complete cds
J6	thioredoxin 2
J7	glycoprotein Ib (platelet), β polypeptide
J8	topoisomerase (DNA) II β
J9	HLA-B associated transcript 2
K1	islet cell autoantigen 1, 69 kDa
K2	heat shock factor binding protein 1
K3	stress-induced-phosphoprotein 1 (Hsp70/Hsp90-organizing protein)
K4	C4 complement protein
K5	18S rRNA
K6	thioredoxin domain containing 1
K7	platelet-activating factor acetylhydrolase α2 subunit (PAF-AH α2)
K8	coagulation factor C homolog (*Limulus polyphemus*)
K9	adenylate kinase 3
L1	glutathione *S*-transferase, θ2
L2	RT1 class Ib gene (Aw2)
L3	proprotein convertase subtilisin/kexin type 3
L4	thioredoxin-like (32 kDa)
L5	blank
L6	glutathione *S*-transferase Yc1 subunit (rats, fetal liver, mRNA, 1052 nt)
L7	DnaJ (Hsp40) homolog, subfamily C, member 7
L8	ligase III, DNA, ATP-dependent
L9	SWI/SNF-related, matrix-associated, actin-dependent regulator of chromatin, subfamily e, member 1

cellular resistance to subsequent lethal stressors. For example, heat and ischemia are well known stimuli that induce the HSP70 family in the central nervous system [22]. In mammals, the HSP70 family is also stimulated by stress mediators such as adrenocorticotropic hormone and catecholamines [3]. Accordingly, expression of the HSP70 family may be associated with stress responses involving

the endocrine, nervous, and immune systems. Glucocorticoid levels also are increased in depressed patients [4] and glucocorticoid receptor function is regulated by HPSs [23]. Thus, further investigation of the relationship between HSPs and psycho-physiological stress in hippocampus should be fruitful. In the present study, for example, we constructed a cDNA microarray focused on genes categorized into 'cell/organism defense', including a number of stress inducible factors such as HSPs, for further molecular studies in animal models of stress-related disorders.

As shown in Fig. 3 C, there was significant correlation between the frequencies of observed ESTs categorized into 'cell/organism defense' and the signal intensities of the spots, suggesting that the profiling of transcripts by ESTs reflects the actual gene expression pattern well. These clone sets allow for the production of large numbers of cDNA microarrays at low cost, permitting the use of large numbers of replicates in gene expression profiling experiments, which should lead to increased data quality. In addition, because many of the cDNAs spotted on our microarrays are not contained on commercial platforms at present, they should provide a unique and useful tool for molecular studies of animal models of stress-related disorders.

Functional analysis of newly discovered genes through this approach might clarify the molecular mechanisms underlying the pathogenesis of stress-related disorders sufficiently to reveal novel therapeutic targets. Integrated information on hippocampus-specific functions and mapping of our ESTs on the human chromosome should complement genetic linkage studies and facilitate positional candidate cloning for the identification of genes of memory-, learning- and stress-related disorders in genetically defined regions.

Acknowledgments

This study was supported by Grants-in-Aid for Scientific Research A-C and for Scientific Research on Priority Areas (C) "Medical Genome Science" from the Japanese Ministry of Science, Education, Sports, Culture and Technology; for a Health and Labor Science Research Grant for Special Research from the Japanese Ministry of Health, Labor and Welfare; and for the Yamanouchi Foundation for Research on Metabolic Disorders, Japan Diabetes Foundation and Takeda Science Foundation.

References

[1] M.D. Adams, A.R. Kerlavage, R.D. Fleischmann, R.A. Fuldner, C.J. Bult, N.K. Lee, E.F. Kirkness, K.G. Weinstock, J.D. Gocayne, O. White, et al., Initial assessment of human gene diversity and expression patterns based upon 83 million nucleotides of cDNA sequence, Nature 377 (1995) 3–174 (Suppl.).

[2] S.F. Altschul, T.L. Madden, A.A. Schäffer, J. Zhang, Z. Zhang, W. Miller, D.J. Lipman, Gapped BLAST and PSI-BLAST: a new generation of protein database search programs, Nucleic Acids Res. 25 (1997) 3389–3402.

[3] M.J. Blake, D.J. Buckley, A.R. Buckley, Dopaminergic regulation of heat shock protein-70 expression in adrenal gland and aorta, Endocrinology 132 (1993) 1063–1070.

[4] B.J. Carroll, The dexamethasone suppression test for melancholia, Br. J. Psychiatry 140 (1982) 292–304.

[5] N.A. Datson, J. van der Perk, E.R. de Kloet, E. Vreugdenhil, Expression profile of 30,000 genes in rat hippocampus using SAGE, Hippocampus 11 (2001) 430–444.

[6] R.S. Duman, J. Malberg, J. Thome, Neural plasiticity to stress and antidepressant treatment, Biol. Psychiatry 46 (1999) 1181–1191.

[7] P.S. Eriksson, E. Perfilieva, T. Bjork-Eriksson, A.M. Alborn, C. Nordborg, D.A. Peterson, F.H. Gage, Neurogenesis in the adult human hippocampus, Nat. Med. 4 (1998) 1313–1317.

[8] E. Fuchs, G. Flugge, Stress, glucocorticoids and structural plasticity of the hippocampus, Neurosci. Biobehav. Rev. 23 (1998) 295–300.

[9] K. Fukunaga, L. Stoppini, E. Miyamoto, D. Muller, Long-term potentiation is associated with an increased activity of Ca^{2+}/calmodulin-dependent protein kinase II, J. Biol. Chem. 268 (1993) 7863–7867.

[10] R.A. Gibbs, G.M. Weinstock, M.L. Metzker, D.M. Muzny, E.J. Sodergren, S. Scherer, G. Scott, D. Steffen, K.C. Worley, P.E. Burch, et al., Genome sequence of the Brown Norway rat yields insights into mammalian evolution, Nature 428 (2004) 493–521.

[11] E. Gould, P. Tanapat, Stress and hippocampal neurogenesis, Biol. Psychiatry 46 (1999) 1472–1479.

[12] J.P. Herman, M.K. Schafer, E.A. Young, R. Thompson, J. Douglass, H. Akil, S.J. Watson, Evidence for hippocampal regulation of neuroendocrine neurons of the hypothalamo–pituitary–adrenocortical axis, J. Neurosci. 9 (1989) 3072–3082.

[13] D.M. Hwang, A.A. Dempsey, R.X. Wang, M. Rezvani, J.D. Barrans, et al., A genome-based resource for molecular cardiovascular medicine. Toward a compendium of cardiovascular genes, Circulation 96 (1997) 4146–4203.

[14] T. Ichimura, T. Isobe, T. Okuyama, T. Yamauchi, H. Fujisawa, Brain 14-3-3 protein is an activator protein that activates tryptophan 5-monooxygenase and tyrosine 3-monooxygenase in the presence of Ca^{2+}, calmodulin-dependent protein kinase II, FEBS Lett. 13 (1987) 79–82.

[15] L. Jin, H. Wang, T. Narita, R. Kikuno, O. Ohara, N. Shihara, T. Nishigori, Y. Horikawa, J. Takeda, Expression profile of mRNAs from human pancreatic islet tumors, J. Mol. Endocrinol. 31 (2003) 519–528.

[16] E.R. Kandel, The molecular biology of memory storage: a dialogue between genes and synapses, Science 294 (2001) 1030–1038.

[17] E.H. Margulies, S.L.R. Kardia, J.W. Innis, Identification and prevention of a GC content bias in SAGE libraries, Nucleic Acids Res. 29 (12) (2001) E60-0.

[18] A. Matynia, S.G. Angnostaras, A.J. Silva, Weaving the molecular and cognitive strands of memory, Neuron 32 (2001) 557–559.

[19] M. Mayford, J. Wang, E. Kandel, T.S. O'Dell, CAMK II regulates the frequency–response function of hippocampal synapses for the production of both LTD and LTP, Cell 81 (1995) 891–904.

[20] B.S. McEwen, The neurobiology of stress: from serendipity to clinical relevance, Brain Res. 886 (2000) 172–189.

[21] M. Nilsson, E. Perfilieva, U. Johansson, O. Orwar, P.S. Eriksson, Enriched environment increases neurogenesis in the adult rat dentate gyrus and improves spatial memory, J. Neurobiol. 39 (1999) 569–578.

[22] T.S. Nowak Jr., U. Bond, M.J. Schlesinger, Heat shock RNA levels in brain and other tissues after hyperthermia and transient ischemia, J. Neurochem. 54 (1990) 451–458.

[23] W.B. Pratt, D.O. Tort, Steroid receptor interactions with heat shock protein and immunophilin chaperones, Endocr. Rev. 18 (1997) 306–360.

[24] R.M. Sapolsky, Glucocorticoids and hippocampal atrophy in neuropsychiatric disorders, Arch. Gen. Psychiatry 57 (2000) 925–935.

[25] Y.I. Sheline, P.W. Wang, M.H. Gado, J.G. Csernansky, M.W. Vannier, Hippocampal atrophy in recurrent major depression, Proc. Natl. Acad. Sci. U. S. A. 93 (1996) 3908–3913.
[26] A.C. Silva, C. Stevens, S. Tonegawa, Y. Wang, Deficient hippocampal long-term potentination in α-calcium-calmodulin kinase II mutant mice, Science 257 (1992) 201–206.
[27] J.D. Sweatt, The neuronal MAP kinase cascade: a biochemical signal integration system subserving synaptic plasticity and memory, J. Neurochem. 76 (2001) 1–10.
[28] J. Takeda, H. Yano, S. Eng, G.I. Bell, A molecular inventory of human pancreatic islets: sequence analysis of 1000 cDNA clones, Hum. Mol. Genet. 2 (1993) 1793–1798.
[29] H. van Praag, G. Kempermann, F.H. Gage, E. Gould, P. Tanapat, Running increase cell prolification and neurogenesis in the adult mouse dentate gyrus, Nat. Neurosci. 2 (1999) 266–270.
[30] E.A. Young, R.F. Haskett, V. Murphy-Weinberg, S.J. Watson, H. Akil, Loss of glucocorticoid fast feedback in depression, Arch. Gen. Psychiatry 48 (1991) 693–699.

Available online at www.sciencedirect.com
SCIENCE DIRECT®
Biochemical and Biophysical Research Communications 321 (2004) 510–513
BBRC
www.elsevier.com/locate/ybbrc

Acute effect of corticosterone on *N*-methyl-D-aspartate receptor-mediated Ca^{2+} elevation in mouse hippocampal slices

Satoru Sato [a], Hiromi Osanai [a], Toshihiro Monma [a], Tokiko Harada [a], Ayumi Hirano [a], Minoru Saito [a,*], Suguru Kawato [b]

[a] *Department of Physics and Applied Physics, College of Humanities and Sciences, Nihon University, 3-25-40 Sakurajosui, Setagaya-ku, Tokyo 156-8550, Japan*
[b] *Department of Biophysics and Life Sciences, Graduate School of Arts and Sciences, University of Tokyo at Komaba, Tokyo 153-8902, Japan*

Received 10 June 2004

Abstract

We examined the rapid effects of corticosterone (CORT) on *N*-methyl-D-aspartate (NMDA) receptor-mediated Ca^{2+} signals in adult mouse hippocampal slices by using Ca^{2+} imaging technique. Application of NMDA caused a transient elevation of intracellular Ca^{2+} concentration followed by a decay to a plateau within 150 s. The 30 min preincubation of CORT induced a significant decrease of the peak amplitude of NMDA-induced Ca^{2+} elevation in the CA1 region. The rapid effect of CORT was induced at a stress-induced level (0.4–10 μM). Because the membrane non-permeable bovine serum albumin-conjugated CORT also induced a similar rapid effect, the rapid effect of CORT might be induced via putative surface CORT receptors. In contrast, CORT induced no significant effects on NMDA-induced Ca^{2+} elevation in the dentate gyrus. In the CA3 region, CORT effects were not evaluated, because the marked elevation of NMDA-induced Ca^{2+} signals was not observed there.

Keywords: Acute effect; Ca^{2+} signals; Corticosterone; Glucocorticoids; NMDA receptor; Hippocampus

Corticosterone (CORT) is a principal glucocorticoid synthesized in the rodent adrenal cortex and secreted in response to stress. There are a series of studies about the chronic and genomic effects of corticosteroids in the hippocampus [1,2]. The stress-induced increase in CORT secretion is known to produce neuronal cell damage. Exogenous application of a high dose of CORT has been shown to elicit the neuronal atrophy in the hippocampus [3]. Rats exposed to restraint stress for three weeks exhibited neuronal atrophy identical to that seen in rats treated with a high dose of CORT for three weeks [4]. In addition to these classical genomic effects, which are actuated via intracellular steroid receptors, glucocorticoids act acutely on neuronal excitability [5,6]. The long-term potentiation (LTP) of the population spike amplitude was also acutely (within 1 h) suppressed by a high concentration of glucocorticoids [7]. It has also been demonstrated that CORT dosage for 20 min significantly suppresses the development of LTP in the CA1 region of 4-week-old rat hippocampal slices [8,9].

It is well known that Ca^{2+} influx via *N*-methyl-D-aspartate (NMDA) receptors plays a crucial role in the induction of LTP. The rapid effects of CORT (appearing within 30 min) on NMDA-induced Ca^{2+} signal transduction, however, have not been well elucidated in the hippocampus. In the present study, we examined the rapid effects of CORT on NMDA receptor-mediated Ca^{2+} signals in mouse hippocampal slices by using Ca^{2+} imaging technique. An advantage of mouse hippocampal slices was that we could measure the CA1, CA3, and dentate gyrus regions simultaneously because the whole hippocampus fell within the microscope field. As a

* Corresponding author. Fax: +81-3-5317-9432.
E-mail address: msaito@chs.nihon-u.ac.jp (M. Saito).

0006-291X/$ - see front matter © 2004 Elsevier Inc. All rights reserved.
doi:10.1016/j.bbrc.2004.06.168

result, the 30 min preincubation of CORT induced a significant decrease of the peak amplitude of NMDA-induced Ca^{2+} elevation in the CA1 region. The rapid effect of CORT region was induced at a stress-induced level (0.4–10 μM). In contrast, CORT induced no significant effects on NMDA-induced Ca^{2+} elevation in the dentate gyrus. In the CA3 region, CORT effects were not evaluated, because the marked elevation of NMDA-induced Ca^{2+} signals was not observed there.

Materials and methods

Brain slices (coronal, 300 μm thick) were prepared from 7-week-old male ddY mice after exposure to an overdose of diethyl ether anesthesia. In order to stabilize the plasma glucocorticoid level, mice used in all experiments were decapitated at the same moment (10 a.m.) in the circadian cycle. Following decapitation, the brain was quickly removed and placed in ice-cold oxygenated artificial cerebrospinal fluid (ACSF) (composition in mM: NaCl 124, KCl 5, $CaCl_2$ 2, $NaHCO_3$ 22, $MgSO_4$ 2, NaH_2PO_4 1.24, glucose 10, pH 7.4, and bubbled with 95% O_2/5% CO_2). Slices were then prepared using a microslicer (DTK-1000; Dosaka-EM, Kyoto, Japan). The slices were recovered in ACSF at 30 °C for 60 min and held at room temperature until use. All experiments using animals were conducted in accordance with the institutional guidelines.

Measurement of intracellular Ca^{2+} concentration $[Ca^{2+}]_i$ was performed using the Ca^{2+}-sensitive indicator fura-2. Prior to Ca^{2+} signal measurements, the slices were loaded for 30 min at room temperature with 10 μM fura-2/AM [from 1 mM stock solution in dimethyl sulfoxide (DMSO)] in the presence of 0.01% cremophore EL in 7.2 mL ACSF. After loading with fura-2, the slices were washed in ACSF for 30 min and then preincubated with CORT or bovine serum albumin-conjugated CORT (BSA–CORT) solution for 30 min. CORT and BSA–CORT solutions were prepared at the appropriate dilution with low Mg^{2+} ACSF (control solution) (composition in mM: NaCl 124, KCl 5, $CaCl_2$ 2, $NaHCO_3$ 22, $MgSO_4$ 0.1, NaH_2PO_4 1.24, glucose 10, pH 7.4, and gassed with 5% CO_2/95% O_2) from the stock solution in DMSO. The final concentration of DMSO was less than 0.05% in each case.

For fluorescence measurements of $[Ca^{2+}]_i$, a digital fluorescence microscope system, consisting of an inverted microscope (TE 300; Nikon, Tokyo, Japan) equipped with a xenon lamp for excitation and a CCD camera (C4742-95; Hamamatsu Photonics, Hamamatsu, Japan), was used. Preincubated brain slices were placed in a chamber on the microscope stage. The whole hippocampus fell within the microscope field by using a 4× fluorescence objective (Nikon, Tokyo, Japan). The slices were then perfused with the CORT or BSA–CORT solution kept at 30 °C. At 150 s after the onset of recording the perfusing solution was replaced by the solution containing 1 mM NMDA.

For fura-2 measurements, the excitation wavelength varied discretely between 340 and 380 nm, and $[Ca^{2+}]_i$ was expressed as F340/F380, which is the ratio of the 510 nm fluorescence intensity at 340 nm excitation (F340) to that at 380 nm excitation (F380). In each acquisition trial, consecutive fluorescence images were acquired at 5 s intervals for 350 s. Fig. 1 shows examples of a series of obtained images. The fluorescence images were then analyzed with AQUACOSMOS system (Ver.1.3; Hamamatsu Photonics, Hamamatsu, Japan). Twelve ROIs (regions of interest: 5 × 5 pixels) were put on the cell body layer of each hippocampal subfield, and the fluorescence data of those ROIs were averaged.

The data were expressed as means ± SEM. Student's t test was utilized to test the significance of observed differences between groups. Significance was set at $p < 0.005$.

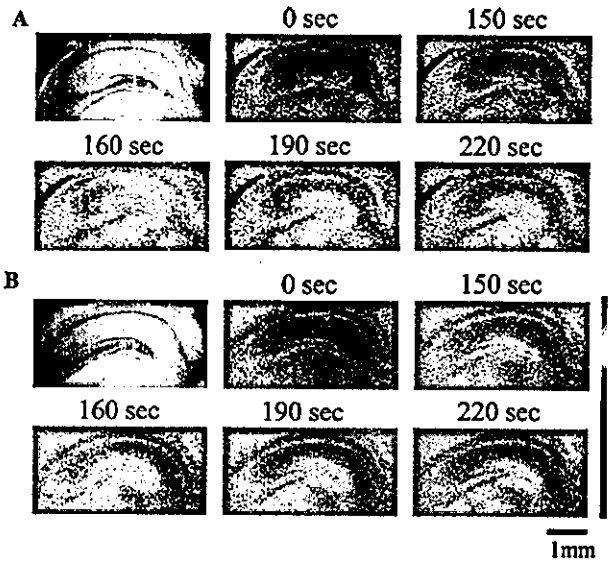

Fig. 1. Fluorescence images of mouse hippocampal slices (A) without the CORT dosage and (B) with the 1 μM CORT dosage. Upper left one of each column is a fluorescence image of a fura-2-loaded slice excited at 380 nm. The other pseudo-colored images demonstrate $[Ca^{2+}]_i$ in the slice. The color bar shows the ratio of the fluorescence intensity of fura-2 excited at 340 and 380 nm, which expresses $[Ca^{2+}]_i$, from blue (low $[Ca^{2+}]_i$) to red (high $[Ca^{2+}]_i$). The time above each pseudo-colored image shows the time from the onset of experiment. At 150 s after the onset of experiment, 1 mM NMDA was applied.

Results

Fig. 2 shows the typical time courses of NMDA-induced Ca^{2+} signal obtained from (A) the CA1 region and (B) the dentate gyrus. The response to continuous NMDA exposure was characterized by a transient elevation in $[Ca^{2+}]_i$ followed by a decay to a plateau within 150 s (see also Fig. 1). The transient elevation in $[Ca^{2+}]_i$ was due to NMDA receptor-mediated Ca^{2+} influx, because no response to NMDA application was observed in the slices preincubated with 100 μM of NMDA antagonist MK-801 (Fig. 2). In the control condition without CORT or BSA–CORT preincubation, the peak amplitudes of $[Ca^{2+}]_i$ elevation, calculated as an increase (Δ(F340/F380)) in F340/F380 from baseline level, were 0.40 ± 0.03 ($n = 7$) in the CA1 region, 0.05 ± 0.01 ($n = 7$) in the CA3 region, and 0.22 ± 0.01 ($n = 7$) in the dentate gyrus. These average values were set to 100%. In the CA1 region, the peak amplitude of $[Ca^{2+}]_i$ elevation was decreased by preincubation with CORT in a dose-dependent manner. The decreased peak amplitudes were $49.4 \pm 9.9\%$ ($n = 5$, $p < 0.005$), $43.0 \pm 7.7\%$ ($n = 9$), and $30.4 \pm 2.0\%$ ($n = 5$) at 0.4, 1, and 10 μM of CORT compared with control (Fig. 3A). In addition, preincubation with 1 μM BSA–CORT (approximately 20 CORT molecules per BSA molecule) also induced a decrease in the peak amplitude ($30.2 \pm 5.0\%$, $n = 5$, $p <$ 0.005). In contrast,

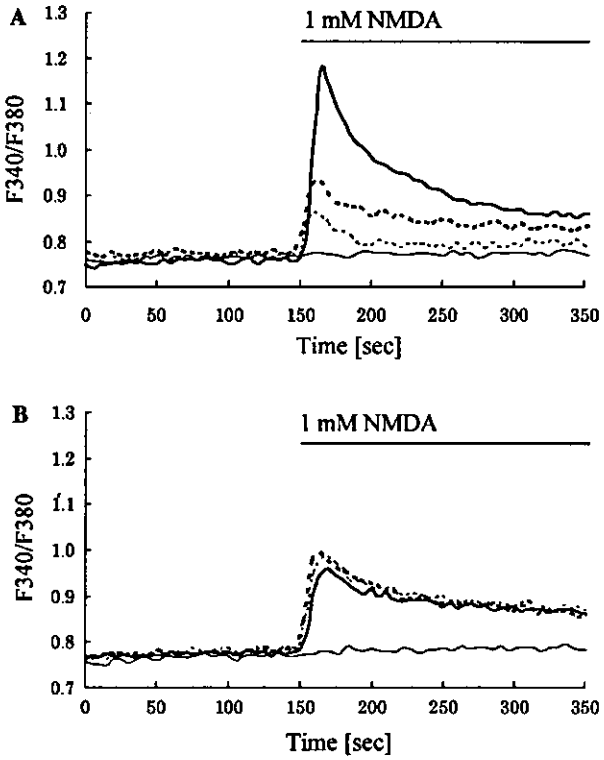

Fig. 2. Typical time courses of NMDA-induced Ca^{2+} signal in (A) the CA1 region and (B) the dentate gyrus. The vertical scale (F340/F380) is the ratio of the fluorescence intensity of fura-2 excited at 340 and 380 nm. Without the CORT dosage, 1 mM NMDA application induced a transient elevation in $[Ca^{2+}]_i$ followed by a decay to a plateau (control: thick line). The Ca^{2+} signal almost disappeared with the 100 μM MK-801 dosage (thin line). With the dosage of CORT, the $[Ca^{2+}]_i$ elevation was decreased compared with control in the CA1 region (1 μM CORT, thick-dotted line; 10 μM CORT, thin-dotted line). In contrast, the CORT dosage induced no significant effect on the Ca^{2+} signal in the dentate gyrus.

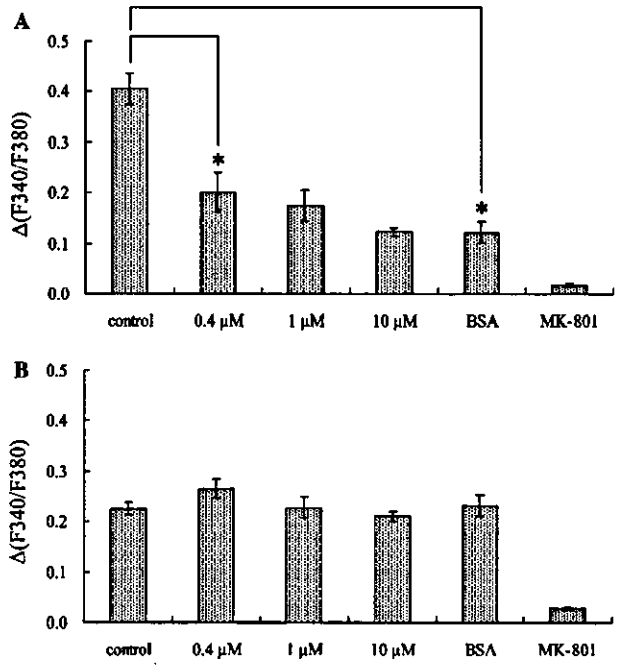

Fig. 3. The effect of CORT on the peak amplitude of NMDA-induced Ca^{2+} signal elevation in (A) the CA1 region and (B) the dentate gyrus. The vertical scale (Δ(F340/F380)) is the peak amplitude of F340/F380 from baseline. The concentrations below the figures show the dosed concentrations of CORT. BSA and MK-801 show the dosage of 1 μM BSA–CORT and 100 μM MK-801, respectively. The data are expressed as means ± SEM. The $[Ca^{2+}]_i$ elevation was significantly suppressed at 0.4 μM CORT and 1 μM BSA–CORT in the CA1 region. $^*p < 0.005$ compared from control value.

preincubation with neither CORT nor BSA–CORT significantly changed the peak amplitude of $[Ca^{2+}]_i$ elevation in the dentate gyrus: the peak amplitudes were 117.8 ± 8.5% ($n = 5$), 101.1 ± 9.4% ($n = 9$), and 93.5 ± 4.6% ($n = 5$) at 0.4, 1, and 10 μM of CORT, and 103.2 ± 9.1% ($n = 5$) at 1 μM BSA–CORT compared with control (Fig. 3B). In the CA3 region, CORT and BSA-CORT effects were not evaluated, because the marked elevation of NMDA-induced Ca^{2+} signals was not observed there.

Discussion

In the present study, we examined the rapid effects of CORT on NMDA receptor-mediated Ca^{2+} signals in adult mouse hippocampal slices by using Ca^{2+} imaging technique. An advantage of mouse hippocampal slices was that we could measure the CA1, CA3, and dentate gyrus regions simultaneously because the whole hippocampus fell within the microscope field. Concerning rat hippocampal slices, we need to use different slices in order to compare the CA1, CA3, and dentate gyrus regions, resulting in losing accuracy of the relative levels for the $[Ca^{2+}]_i$ elevation. In addition, the heterogeneous effect of CORT between the CA1, CA3, and dentate gyrus regions could not be examined in our previous study using cultured neonatal hippocampal neurons [10], because all the neurons were mixed up there.

The present results showed the rapid effects (within 30 min) on NMDA-induced Ca^{2+} signals particularly in the CA1 region. The transient elevation in $[Ca^{2+}]_i$ induced by NMDA application was significantly suppressed to 49.4% at 0.4 μM CORT in the CA1 region. The increases of CORT concentration to 1.0 and 10 μM gave only a small additional decrease to 43.0 and 30.4%. The CORT effect in the CA1 region is physiologically significant, because rats subjected to immobilization-stress for 1 h were reported to show approximately 2 μM CORT in blood plasma [11]. In our previous study, a similar suppressive effect of CORT was also found in the CA1 region of 4-week-old rat hippocampal slices, in which the peak amplitude of $[Ca^{2+}]_i$ elevation decreased to 79.5% compared with control in the presence of 10 μM CORT (unpublished results).

On the other hand, CORT induced no significant effects on NMDA-induced Ca^{2+} elevation in the dentate gyrus as mentioned above. In the CA3 region, the marked elevation of NMDA-induced Ca^{2+} signals was not observed, although NMDA receptor should also be in the CA3 region. This reason is not clear at this stage.

The rapid effect of CORT on NMDA receptor-mediated Ca^{2+} signals was also found in the cultured neonatal hippocampal neurons in our previous study [10]. It should be noted that in the cultured neonatal hippocampal neurons, CORT induced the extreme prolongation of time duration of NMDA-induced Ca^{2+} elevation. However, the differences in the rapid effect of CORT between the previous study (using dissociated neonatal hippocampal neurons) and the present study (using adult mouse hippocampal slices) may not be controversial, because the age of hippocampal neurons was completely different between these preparations. Different effects of CORT may be due to the differences in molecular types of NMDA receptor subunits which are different between neonatal neurons (containing mainly NR2B) and adult neurons (containing both NR2A and NR2B) [12].

According to the classical view of the steroid action, CORT is thought to penetrate into the cytoplasm of neurons, bind to intracellular receptors, and induce genomic effects through new protein synthesis, resulting in the modulation of Ca^{2+} signals [1–4]. The present results suggested that CORT may bind to putative surface CORT receptors, because the membrane non-permeable BSA–CORT also induced a similar rapid effect. The possibility of genomic mechanisms can be also excluded as an explanation for the present CORT effect, because cycloheximide, an inhibitor of protein synthesis, did not abolish the effect of CORT on NMDA-induced Ca^{2+} signals.

A possible candidate for surface CORT receptors is a classical intracellular glucocorticoid receptor (e.g., GR, a type-2 receptor), which may be bound to plasma membranes. This idea is supported by reports that the immunoreactivity of antibodies against GR was associated with plasma membranes from hippocampal and hypothalamic neurons [13] and that specific CORT binding to neuronal membranes occurred in different brain areas with moderate affinity (K_d = 120 nM) [14,15]. Classical GRs are expressed in the cytoplasm of cultured hippocampal neurons [16]. GRs may drive both classical genomic pathways [17] and non-genomic pathways (the current study) in hippocampal neurons.

It is well known that Ca^{2+} influx via NMDA receptors plays a crucial role in the induction of LTP. The present results may have a good coincidence to the rapid suppressive effect of CORT found by electrophysiological investigations on the LTP in the CA1 region of 4-week-old rat hippocampal slices [8,9].

References

[1] S.M. Nair, T.R. Werkman, J. Craig, R. Finnell, M. Joels, J.H. Eberwine, Corticosteroid regulation of ion channel conductances and mRNA levels in individual hippocampal CA1 neurons, J. Neurosci. 18 (1998) 2685–2696.

[2] L.P. Reagan, B.S. McEwen, Contoversies surrounding glucocorticoid-mediated cell death in the hippocampus, J. Chem. Neuroanat. 13 (1997) 149–167.

[3] C.S. Wooly, E. Gould, B.S. McEwen, Exposure to excess glucocorticoids alters dendritic morphology of adult hippocampal pyramidal neurons, Brain Res. 531 (1990) 225–231.

[4] Y. Watanabe, E. Gould, B.S. McEwen, Stress induces atrophy of apical dendrites of hippocampal CA3 pyramidal neurons, Brain Res. 588 (1992) 341–345.

[5] P.W. Landfield, T.A. Pitler, Prolonged Ca^{2+} dependent after hyper-polarizations in hippocampal neurons of aged rats, Science 226 (1984) 1089–1092.

[6] S.J. Lupien, B.S. McEwen, The acute effect of corticosteroids on cognition: integration of animal and human model studies, Brain Res. Rev. 24 (1997) 1–27.

[7] C. Vidal, W. Jordan, W. Zieglgansberger, Corticosterone reduces the excitability of hippocampal pyramidal cells in vitro, Brain Res. 383 (1986) 54–59.

[8] S. Kawato, M. Yamada, T. Kimoto, Neurosteroids are 4th generation neuromessengers: cell biophysical analysis of steroid transduction, Adv. Biophys. 37 (2001) 1–30.

[9] K. Shibuya, N. Takata, Y. Hojo, A. Furukawa, N. Yasumasu, T. Kimoto, T. Enami, K. Suzuki, N. Tanabe, H. Ishii, H. Mukai, T. Takahashi, T. Hattori, S. Kawato, Hippocampal cytochrome P450s synthesize brain neurosteroids which are paracrine neuromodulators of synaptic signal transduction, Biochim. Biopys. Acta 1619 (2003) 301–316.

[10] T. Takahashi, T. Kimoto, N. Tanabe, T. Hattori, N. Yasumatsu, S. Kawato, Corticosterone acutely prolonged *N*-methyl-D-aspartate receptor-mediated Ca^{2+} elevation in cultured rat hippocampal neurons, J. Neurochem. 83 (2002) 1441–1451.

[11] S. Marinesco, C. Bonnet, R. Cespuglio, Influence of stress duration on the sleep rebound induced by immobilization in the rat: a possible role for corticosterone, Neuroscience 92 (1999) 921–933.

[12] H. Monyer, N. Burnashev, D.J. Laurie, B. Sakmann, P.H. Seeburg, Developmental and regional expression in the rat brain and functional properties of four NMDA receptors, Neuron 12 (1994) 529–540.

[13] Z. Lipositz, M.C. Bohn, Association of glucocorticoid receptor immunoreactivity with cell membrane and transport vesicles in hippocampal and hypothalamic neurons of the rat, J. Neurosci. Res. 35 (1993) 14–19.

[14] A.C. Towle, P.Y. Sze, Steroid binding to synaptic plasma membrane: differential binding of glucocorticoids and gonadal steroids, J. Steroid Biochem. 18 (1983) 135–143.

[15] Z. Guo, Y.Z. Chen, R.B. Xu, H. Fu, Binding characteristics of glucocorticoid receptor in synaptic plasma membrane from rat brain, Funct. Neurol. 10 (1995) 183–194.

[16] D.R. Packan, R.M. Sapolsky, Glucocorticoid endangerment of the hippocampus: tissue, steroid and receptor specificity, Neuroendocrinology 51 (1990) 613–618.

[17] M. Nishi, H. Ogawa, T. Ito, K.I. Matsuda, M. Kawata, Dynamic changes in subcellular localization of mineralocorticoid receptor in living cells: in comparison with glucocorticoid receptor using dual-color labeling with green fluorescent protein spectral variants, Mol. Endocrinol. 15 (2001) 1077–1092.

Adult male rat hippocampus synthesizes estradiol from pregnenolone by cytochromes P45017α and P450 aromatase localized in neurons

Yasushi Hojo*†, Taka-aki Hattori*†, Taihei Enami*, Aizo Furukawa†‡, Kumiko Suzuki*, Hiro-taka Ishii*, Hideo Mukai*†, John H. Morrison§, William G. M. Janssen§, Shiro Kominami¶, Nobuhiro Harada‖, Tetsuya Kimoto*†, and Suguru Kawato*†**

*Department of Biophysics and Life Sciences and †Core Research for Evolutional Science and Technology Project of Japan Science and Technology Corporation, Graduate School of Arts and Sciences, University of Tokyo at Komaba, Meguro, Tokyo 153, Japan; ‡Department of Psychiatry, Tokyo Metropolitan Matsuzawa Hospital, 2-1-1 Kamikitazawa, Setagaya, Tokyo 156, Japan; §Kastor Neurobiology of Aging Laboratories, Fishberg Research Center for Neurobiology, Mount Sinai School of Medicine, New York, NY 10029; ¶Faculty of Integrated Arts and Sciences, Hiroshima University, Higashi-hiroshima 739, Japan; and ‖Department of Biochemistry, School of Medicine, Fujita Health University, Toyoake, Aichi 470, Japan

Edited by Bruce S. McEwen, The Rockefeller University, New York, NY, and approved October 16, 2003 (received for review March 5, 2003)

In adult mammalian brain, occurrence of the synthesis of estradiol from endogenous cholesterol has been doubted because of the inability to detect dehydroepiandrosterone synthase, P45017α. In adult male rat hippocampal formation, significant localization was demonstrated for both cytochromes P45017α and P450 aromatase, in pyramidal neurons in the CA1–CA3 regions, as well as in the granule cells in the dentate gyrus, by means of immunohistochemical staining of slices. Only a weak immunoreaction of these P450s was observed in astrocytes and oligodendrocytes. ImmunoGold electron microscopy revealed that P45017α and P450 aromatase were localized in pre- and postsynaptic compartments as well as in the endoplasmic reticulum in principal neurons. The expression of these cytochromes was further verified by using Western blot analysis and RT-PCR. Stimulation of hippocampal neurons with *N*-methyl-D-aspartate induced a significant net production of estradiol. Analysis of radioactive metabolites demonstrated the conversion from [^{3}H]pregnenolone to [^{3}H]estradiol through dehydroepiandrosterone and testosterone. This activity was abolished by the application of specific inhibitors of cytochrome P450s. Interestingly, estradiol was not significantly converted to other steroid metabolites. Taken together with our previous finding of a P450scc-containing neuronal system for pregnenolone synthesis, these results imply that 17β-estradiol is synthesized by P45017α and P450 aromatase localized in hippocampal neurons from endogenous cholesterol. This synthesis may be regulated by a glutamate-mediated synaptic communication that evokes Ca^{2+} signals.

The hippocampal formation, essentially involved in learning and memory processes, is known to be a target for the neuromodulatory actions of hormones produced in the gonads. As both estradiol and testosterone may reach the brain via blood circulation, and extensive studies have been performed to investigate their role in modulating hippocampal plasticity and function (1–4). Evidence is emerging that estrogen exerts not only the chronic/genomic effects but also a rapid/nongenomic influence on hippocampal synaptic plasticity (2, 5). In addition to endocrine-derived hormones, recent experiments have demonstrated that hippocampal neurons may also be exposed to locally synthesized brain neurosteroids, such as pregnenolone (PREG) and its sulfated ester (6–9). Dehydroepiandrosterone (DHEA) has been found in the mammalian brain at concentrations greater than that in plasma (6, 10). Because DHEA concentrations do not decrease after adrenalectomy and castration, many experiments have been performed with the aim of demonstrating the *de novo* synthesis of DHEA within the brain. DHEA biosynthesis has been demonstrated in cultured glial cells and neurons from the neonatal rat brain (11, 12). In the adult brain, however, a concrete demonstration of the synthesis of DHEA, androstenedione (AD), testosterone, or estradiol directly from endogenous cholesterol has yet to be reported. Sex steroids such as estradiol and testosterone, therefore, have not classically been considered to be "brain-derived neurosteroids." Furthermore, the localization and activity of cytochrome P45017α (CYP17) in adult mammalian brain has also not been demonstrated, despite many sophisticated studies employing immunohistochemistry, molecular biology, and enzyme activity assays (13–16). P45017α has, therefore, been regarded to be only transiently expressed in the brain at embryonic and neonatal stages (11, 12, 14). Recently, a few studies have reported the presence of cytochrome P450 aromatase (P450arom, CYP19) in the adult rat and human hippocampal formation (17, 18).

The present study was designed to examine, in the adult male hippocampus, the cellular localization of P45017α and P450arom and the endogenous metabolism of neurosteroids from PREG. Analyses revealed the neuronal localization of these P450s and the synthesis of DHEA, testosterone, and 17β-estradiol, which suggests their intracrine/paracrine actions on the plasticity of neurons in adult rat brain.

Materials and Methods

Animals. Adult male Wistar rats (3 months old, 210–250 g) were purchased from SLC Japan and Harlan Sprague–Dawley. All experiments using animals in this study were conducted according to the institutional guidelines.

Immunohistochemical Staining of Hippocampal Slices. Immunohistochemical staining was performed essentially as described in refs. 7 and 8. The hippocampi were frozen-sliced with a cryostat. After application of either anti-P45017α IgG (19), at 1/1,000 dilution or anti-P450arom IgG (20) at 1/1,000, the slices were incubated for 18–36 h. Biotinylated anti-rabbit IgG and streptavidin–horseradish peroxidase complex (Vector Laboratories) was applied. Immunoreactive cells were detected in diaminobenzidine-nickel. Fluorescence immunohistochemistry was performed by using streptavidin–Oregon Green 488. For detailed description of the procedures, see *Supporting Text*, which is published as supporting information on the PNAS web site.

Postembedding ImmunoGold Method for Electron Microscopy. Hippocampal slices were prepared by using a vibratome. Freeze substitution and low-temperature embedding of the specimens was performed as described (21). Slices were plunged into liquid propane and immersed in uranyl acetate solution. After polymerization of Lowicryl HM20 resin, ultrathin sections (80 nm

This paper was submitted directly (Track II) to the PNAS office.

Abbreviations: PREG, pregnenolone; DHEA, dehydroepiandrosterone; AD, androstenedione; P450arom, cytochrome P450 aromatase; 17β-HSD, 17β-hydroxysteroid dehydrogenase; DHT, dihydrotestosterone.

**To whom correspondence should be addressed. E-mail: kawato@phys.c.u-tokyo.ac.jp.